

Improved white dwarves constraints on inelastic dark matter and left-right symmetric models

Anirban Biswas^{1,2,*} Arpan Kar^{1,2,†} Hyomin Kim^{1,2,‡} Stefano Scopel^{1,2,§} and Liliana Velasco-Sevilla^{1,2,3,||}

¹Center for Quantum Spacetime, Sogang University, Seoul 121-742, South Korea

²Department of Physics, Sogang University, Seoul 121-742, South Korea

³Korea Institute for Advanced Study, Seoul 02455, South Korea



(Received 28 July 2022; accepted 12 September 2022; published 18 October 2022)

Weakly interacting massive particles (WIMPs) can be captured in compact stars such as white dwarves (WDs) if they are in a dark matter (DM)-rich environment, leading to an increase in the star luminosity through their annihilation process. N -body simulations suggest that the core of the Messier 4 globular cluster (where plenty of WDs are observed) is rich of DM. Assuming this is the case, we use a recent improvement in the calculation of the WD equation of state to show that when the WIMP interacts with the nuclear targets within the WD through inelastic scattering, and its mass exceeds a few tens of GeV, the data on low-temperature large-mass WDs in M4 can probe values of the mass splitting as large as $\delta \lesssim 40$ MeV. Such value largely exceeds those ensuing from direct detection and from solar neutrino searches. We apply such improved constraint to the specific DM scenario of a self-conjugate bidoublet in the left-right symmetric model (LRSM), where the standard $SU(2)_L$ group with coupling g_L is extended by an additional $SU(2)_R$ with coupling g_R in order to explain maximal parity violation in weak interactions. We show that bounds from WDs significantly reduce the cosmologically viable parameter space of such scenario, in particular requiring $g_R > g_L$. For instance, for $g_R/g_L = 1.8$ we find the two viable mass ranges $1.2 \text{ TeV} \lesssim m_\chi \lesssim 3 \text{ TeV}$ and $5 \text{ TeV} \lesssim m_\chi \lesssim 10 \text{ TeV}$, when the charged $SU(2)_R$ gauge boson mass M_{W_2} is lighter than $\simeq 12 \text{ TeV}$. We also discuss the ultraviolet completion of the LRSM model, when the latter is embedded in a grand unified theory. We show that such low-energy parameter space and compatibility to proton-decay bounds require a nontrivial extension of the particle content of the minimal model. We provide a specific example where $M_{W_2} \lesssim 10 \text{ TeV}$ is achieved by extending the LRSM at high energy with color triplets that are singlets under all other groups, and $g_R/g_L > 1$ is obtained by introducing $SU(2)_L$ triplets with no $SU(2)_R$ counterparts, i.e., by breaking the symmetry between the multiplets of $SU(2)_L$ and $SU(2)_R$.

DOI: [10.1103/PhysRevD.106.083012](https://doi.org/10.1103/PhysRevD.106.083012)

I. INTRODUCTION

The discovery of the nature of cold dark matter (CDM) is one of the most urgent pending issues of modern physics. Weakly interacting massive particles (WIMPs) are the most popular CDM candidates: their mass m_χ falls in the GeV–TeV range and they are expected to have only weak-type interactions with ordinary matter. Such small but non-vanishing interactions keep them in thermal equilibrium in

the Early Universe, providing an expected thermal relic abundance in agreement with observation. They also provide promising signals to detect them: in direct detection (DD) WIMP scattering events off nuclear targets are searched for through the measurement of the ensuing nuclear recoils in low-background detectors (see for instance [1,2]); in accelerators WIMPs can be created from the scattering of Standard Model (SM) initial states (see for instance [3–5]); finally, in indirect detection (ID) the products of the annihilations of DM particles in the halo of our Galaxy or that of dwarf galaxies are searched for both in ground-based and in satellite telescopes (see for example [6–9]).

Annihilation is enhanced wherever the WIMP density is large, so that a peculiar ID signal is provided by celestial bodies such as the Sun or the Earth, that, through the same WIMP–nucleus scattering processes that are searched for in DD, can capture WIMPs developing a high-density population of them in their interior [10–16]. The opacity of the celestial body plasma implies that among the WIMP

*anirban.biswas.sinp@gmail.com

†arpankarphys@gmail.com

‡hyomin1996@naver.com

§scopel@sogang.ac.kr

||liliana.velascosevilla@gmail.com

Published by the American Physical Society under the terms of the [Creative Commons Attribution 4.0 International license](https://creativecommons.org/licenses/by/4.0/). Further distribution of this work must maintain attribution to the author(s) and the published article's title, journal citation, and DOI. Funded by SCOAP³.

annihilation products only neutrinos can escape from its surface, with energies that can reach about one-third of the WIMP mass [17–20]. The detection of neutrinos coming out from the Sun or the Earth with energies ranging from the GeV to the TeV scale would represent a smoking gun of an exotic process, since it could not be explained by any known mechanism [21,22]. The direction of the muons produced by the conversion of such neutrinos in the vicinity of a Cherenkov detector such as Super–Kamiokande or IceCube is strongly correlated to that of the source, providing a powerful background subtraction method [23–25].

Both DD and capture are substantially modified in the scenario of inelastic dark matter (IDM). In this class of models a DM particle χ of mass m_χ interacts with atomic nuclei exclusively by upscattering to a second heavier state χ' with mass $m_{\chi'} = m_\chi + \delta$. A peculiar feature of IDM is that there is a minimal WIMP incoming speed in the target frame matching the kinematic threshold for inelastic upscatters and given by

$$v_{\min}^* = \sqrt{\frac{2\delta}{\mu_{\chi N}}}, \quad (1.1)$$

with $\mu_{\chi N}$ the WIMP-nucleus reduced mass. The WIMP speed in the halo of our Galaxy is bounded by the escape velocity $u_{\text{esc}} \simeq 550$ km/s and for both DD and capture in the Sun or the Earth the targets move in the Galactic rest frame with a relative speed $v_0 \simeq 220$ km/s, corresponding to the rotational curve at the solar system position [26]. As a consequence the WIMP-scattering process in DD vanishes if $v_{\min}^* \gtrsim v_{\max} = u_{\text{esc}} + v_0 \simeq 800$ km/s, because it becomes kinematically not accessible, the incoming WIMP speed being too slow to overcome the inelasticity threshold. Such kinematic bound implies that the largest values of δ that DD can probe are reached by the heaviest targets (xenon, iodine, tungsten) employed in existing experiments and cannot exceed $\delta \simeq 200$ keV [27].

A trivial way to extend the sensitivity to the δ parameter beyond DD is to look for processes where the WIMP scatters off nuclei at higher speeds. For instance, the gravitational potential accelerates the WIMP particles before they scatter off the nuclei of a celestial body, so that their speed can be larger than v_{\max} . Indeed, it can reach 1600 km/s in the center of the Sun, implying that the values of δ that can be probed in IDM by capture can reach $\simeq 600$ keV [28]. As a consequence, for these scenarios the solar capture bounds are stronger than those from DD.

Clearly, even stronger bounds can in principle be obtained from WIMP capture in celestial bodies with a gravitational potential stronger than that of the Sun, such as white dwarves (WDs) [29–31] and neutron stars (NSs) [32,33]. Indeed, in such cases the speed of the scattering WIMP can reach \simeq a few 10^4 km/s (for WDs) [34] or a few 10^5 km/s (for NSs) [35], potentially extending the values

of δ that can be probed up to several tens of MeV for WDs and hundreds of MeV for NSs. WDs have already been used in the literature to put constraints on other DM scenarios [36].

In Ref. [34] the WD equation of state improved in [37] was used to constrain the WIMP-nucleus cross section in the case of elastic scattering. The aim of our paper is to extend the analysis of Ref. [34] to the case of inelastic scattering, showing how this can have dramatic consequences on a specific realization of the IDM scenario, bidoublet DM in left-right symmetric models (LRSM) [38].

In such scenario the DM particle has a nonvanishing hypercharge, leading to a coupling to the Z boson whose size is several orders of magnitude larger than that excluded by DD experiments in the case of elastic scattering. However, it can be reconciled to DD constraints by selecting the parameter space for which the mass splitting $\delta \gtrsim 200$ keV so that the nuclear-scattering process is kinematically forbidden [39]. In particular, for bidoublet DM in the LRSM only DD constraints have been discussed so far. In Sec. III we will update its phenomenological analysis including the improved bound from WDs.

The paper is organized as follows. In Sec. II we extend the WD bounds discussed in [34] to IDM. In particular, in Sec. II A we review the present knowledge on the amount of DM in the globular clusters (GCs) of our Galaxy and specifically in Messier 4 (M4) showing that N -body simulations suggest that it can be large in their core. Based on this assumption, in Sec. II B we will use the data collected by the Hubble Space Telescope on low-temperature WDs in M4 to constraint IDM, showing that indeed it is possible to probe in this way values of δ as large as 30 or 40 MeV. At the end of the same section we also provide a short discussion on how the detection of low-temperature neutron stars could further improve the bounds from WDs to values of the mass splitting δ as large as $\simeq 300$ MeV. In Sec. III we summarize the main features of the bidoublet LRSM model and show how the results of Sec. II B substantially reduce the range of variation of its parameters, in particular requiring a significant splitting at low energy between the couplings g_L and g_R of the two groups $SU(2)_L$ and $SU(2)_R$ in order to yield a thermal relic abundance in agreement with observation. In Sec. III C we discuss the consequences of the results of Sec. III on the running of g_L and g_R and on their unification scale when the LRSM is embedded in a grand unified theory (GUT) and provide a specific realization of such scenario, whose features are given in the Appendix. Finally, Sec. IV contains our conclusions.

II. CONSTRAINTS ON INELASTIC DARK MATTER FROM WHITE DWARVES

A. Dark matter content of the M4 globular cluster

The composition of massive white dwarves is a matter of debate. In particular, recent computations of their interior

suggest that their core could be composed of neon [40]. Depending on the metallicity of their surrounding medium, their chemical composition can also include carbon and oxygen.

They are the most abundant stellar remnants, providing a promising means of probing DM interactions, complementary to terrestrial searches [34,41]. In particular, the core temperature of a WD is too low to ignite nuclear fusion reactions, and as a result, WDs have no internal energy source. On the other hand, compared to the Sun their interior density can be eight orders of magnitude larger [34], while their local environment can be richer in DM particles with a lower velocity dispersion, as is the case for the M4 globular cluster, where low-temperature WDs have been observed [29]. All these features imply that indeed WDs in M4 can capture WIMPs more efficiently than the Sun, and that the DM annihilation process inside the WD can easily dominate its total luminosity, driving its temperature beyond the observed ones. As a consequence, as shown in Sec. II B, the observation of low-temperature WDs in M4 can yield to constraints that are stronger compared to those obtained from WIMP capture in the Sun.

In order to set such limits it is necessary to estimate the DM density surrounding the WDs in the inner region of M4. Unfortunately, direct measurements of the velocity dispersion of stars within globular clusters [42] do not allow to reconstruct their gravitational potential with enough precision to obtain their DM content. As a consequence, one needs to rely on models of GC formation based on N -body simulations [29,43]. This clearly represents the major source of uncertainty in our analysis and other similar ones in the literature. It is fair to say that, for instance, in [44], the presence of DM in GC is referred to as a “controversial” issue, mainly due to the effect of tidal disruption of the host galaxy. However, several analyses suggest that the cores of DM halos in globular clusters should indeed survive successive tidal interactions with the host galaxy. The analysis of the following sections will show that if indeed M4 is rich in DM this can have dramatic consequences on some classes of particle-physics models of dark matter. So, following previous phenomenological analyses [29,34,41] we will assume this possibility. In the present paper we will use the results of [29]. We summarize such results below, addressing the reader to the original literature for further details.

An estimate of the DM content in the M4 GC is obtained in [29] by modeling the GC formation starting from an original DM subhalo of mass $M_{\text{DM}} \simeq 10^7 M_{\odot}$ that falls into our host galactic halo [45]. Once the GC falls into the host halo, mass loss occurs continually through tidal stripping, and the orbit of the subhalo decays down toward the center. Such mass loss can be significant, resulting in only a few percent of the DM of the original subhalo surviving inside the final GC, with a baryon-dominated core with a small mass-to-light ratio that actually resembles those of

observed globular clusters. The presence of baryons in the GC must also be taken into account: on the one hand, in the stellar core it can gravitationally enhance the DM density, while on the other it can reduce it, as a consequence of the heating due to the interaction of DM particles with stars (albeit this latter effect is estimated to be negligible at the radii where WDs are observed within M4). Moreover, when the gas in the original halo which eventually forms the globular cluster loses energy and falls into the core conservation of angular momentum is expected to lead to a contraction of the DM core: also such effect turns out to be negligible at the position where the WDs are observed in M4. Finally, the effect of tidal stripping is taken into account by truncating the density distributions of stars and DM at the tidal radius of the GC. The baryon and DM density profiles within M4 ensuing from such procedure are shown in Fig. 1 of [29], which implies that DM makes up less than $\simeq 40\%$ of the total mass of the cluster, in agreement with observations that indicate a lack of DM in globular clusters. In this sense the authors of [29] consider such estimation to be conservative. In particular, such value corresponds to less than 1% of the original $10^7 M_{\odot}$ halo. Moreover, in Ref. [29] the value of the DM density at the largest radius where WDs within M4 are observed ($\simeq 2.3$ pc, well inside the tidal radius) is estimated to be $\rho_{\text{DM}} \simeq 21 M_{\odot} \text{pc}^{-3} = 798 \text{ GeV cm}^{-3}$. Furthermore, using the baryon and DM density profiles estimated with such procedure a WIMP velocity dispersion of $\simeq 8$ km/s can be obtained by assuming hydrostatic equilibrium and spherical symmetry.

The quantitative estimations of Ref. [29] and summarized in this section will be used in Sec. II B to evaluate the effect of DM capture on the WDs within M4.

B. WIMP capture in white dwarves

Signals generated by pair annihilations of WIMPs captured and accumulated inside the Earth and the Sun have been discussed for a long time [10–13].

In the case of the Earth and the Sun only neutrinos escape from the celestial body, which can be searched for in the upgoing muons flux generated by their conversion in the rock close to a Cherenkov detector. Such signals are sensitive to the yield of the neutrinos produced above the detector’s threshold by the particles produced in the WIMP annihilation, typically fermions or gauge bosons, that are boosted to an energy equal to the WIMP mass before decaying. An exception to this mechanism is provided by light quarks, which are stopped inside the medium before decaying, producing below-threshold neutrinos that are not detectable.

In compact stars such as white dwarves or neutron stars the capture process is analogous. However, in this case the observable effect is an increase of the total luminosity or of the temperature of the star, which depends only on the total electromagnetic energy E_{γ} injected by the annihilation

process. In particular, for the high energies corresponding to the values of the WIMP mass discussed in Sec. III, also the neutrinos produced in the annihilation process are converted into electromagnetic radiation, so that the signal can be practically considered as bolometric and $E_\gamma = 2 m_\chi$.

While crossing a compact star DM particles may get trapped in its gravitational potential, continue to lose energy by scattering against its constituents, and get ultimately captured. A DM particle χ (of mass m_χ) can undergo an inelastic transition to a second heavier state (say, χ') by scattering against a nucleus (of mass m_N) present inside the star if the total kinetic energy in the DM-nucleus center of mass frame is larger than the mass difference δ between the DM particle and the heavier state [28,46–48], i.e.,

$$\frac{1}{2}\mu_{\chi N}w^2 > \delta, \quad (2.1)$$

which is equivalent to Eq. (1.1). The quantity w , which is the speed of the DM particle at a radial distance r from the center of the star, is given by

$$w(r) = \sqrt{u^2 + v_{\text{esc}}(r)^2}, \quad (2.2)$$

where $v_{\text{esc}}(r)$ is the local escape velocity from the star at radius r and u is the asymptotic speed of the DM particles far away from the star.

Considering the WD stars in a nearby globular cluster such as M4, a common choice for the distribution of the speed u in the cluster is a boosted Maxwell Boltzmann (MB) one, which in the reference frame of a WD can be expressed as

$$f(u) = \frac{u}{v_d v_*} \sqrt{\frac{3}{2\pi}} \left(\exp\left[-\frac{3}{2v_d^2}(u - v_*)^2\right] - \exp\left[-\frac{3}{2v_d^2}(u + v_*)^2\right] \right), \quad (2.3)$$

where v_* and v_d are the velocity of the WD and the velocity dispersion of DM inside the globular cluster, respectively. Following [29,34], we have assumed conservative values for v_* and v_d , which are $v_* = 20$ km/s and $v_d = 8$ km/s for the WDs in M4.

Given the density profiles of nuclear elements in a WD, one can estimate the corresponding escape velocity profile $v_{\text{esc}}(r)$. In particular, the authors of Ref. [34] have used an improved equation of state for WDs and calculated the density profiles of thermal electrons and nuclear ions for WDs with different configurations that are made of elements like carbon, oxygen, etc. In particular, assuming that the vast majority of heavier WDs are made of carbon, oxygen, or neon, carbon provides the lowest rate for a

spin-independent (SI) cross section that scales with the atomic mass number squared. Indeed, this is the most common type of interaction expected for WIMPs with nuclei, and it arises in the specific scenario analyzed in Sec. III, so in the following we will assume that the WDs are entirely made of carbon to get conservative bounds. Among the various benchmarks for carbon WD tabulated in [34] we take the heaviest WDs with masses $M_* = 1.38 M_\odot$ and $1.25 M_\odot$ and extract the associated radial profiles for the nuclear density and the escape velocity. The corresponding radii of these two benchmark WDs are $R_* \simeq 1.25 \times 10^3$ km and $R_* \simeq 3.29 \times 10^3$ km, respectively.

For the heaviest WD considered here, the escape velocity v_{esc} in the interior of the star can reach a very high value $\sim 0.1 c$ [34], which in turn extends the kinematic upper limit [shown in Eq. (2.1)] on δ up to several tens of MeV. Due to this reason, using heavier WDs it is possible to probe a high value of δ , as will be described in detail in this subsection.

In the optically thin limit, DM particles crossing a WD can become gravitationally bound to the star after a single scattering. In this case, the rate of DM capture through inelastic scattering is given by [28,46–48]

$$C_{\text{opt-thin}} = \frac{\rho_\chi}{m_\chi} \int_0^{R_*} dr 4\pi r^2 \int_0^\infty du \frac{f(u)}{u} w \Omega(w, r) \times \Theta\left(\frac{1}{2}\mu_{\chi N}w^2 - \delta\right). \quad (2.4)$$

Here ρ_χ is the density of DM at the location of the WD inside the globular cluster. As discussed in Sec. II A, in the local environment of the WDs inside M4 we take $\rho_\chi = 798$ GeV cm⁻³. Note that the Θ function in Eq. (2.4) ensures that the capture rate goes to zero if the condition given in Eq. (2.1) is violated. The interaction rate $\Omega(w, r)$ can be obtained using the following expression:

$$\Omega(w, r) = \eta_N(r) w \Theta(E_{\text{max}} - E_{\text{cap}}) \times \int_{E_{\text{min}}}^{E_{\text{max}}} dE \frac{d\sigma[\chi + N \rightarrow \chi' + N]}{dE} \Theta(E - E_{\text{cap}}), \quad (2.5)$$

where $\eta_N(r)$ is the number density distribution (extracted from [34] for the two benchmark WDs considered) of the target nuclear ion (in our case ¹²C) in the WD, and $\frac{d\sigma[\chi + N \rightarrow \chi' + N]}{dE}$ is the differential cross section (as a function of the recoil energy E) for the DM-nucleus inelastic scattering $\chi + N \rightarrow \chi' + N$. The minimum and the maximum recoil energies (i.e., E_{min} and E_{max}) corresponding to this scattering process and the minimum energy transfer E_{cap} required for the capture [i.e., to scatter a DM particle from w to a velocity less than $v_{\text{esc}}(r)$] are

$$E_{\min,\max} = \frac{1}{2}m_\chi w^2 \left[1 - \frac{\mu_{\chi N}^2}{m_N^2} \left(1 \pm \frac{m_N}{m_\chi} \sqrt{1 - \frac{\delta}{\mu_{\chi N} w^2 / 2}} \right)^2 \right] - \delta,$$

$$E_{\text{cap}} = \frac{1}{2}m_\chi u^2 - \delta. \quad (2.6)$$

In Eq. (2.5) the first Heaviside step function Θ imposes the condition $E_{\max} > E_{\text{cap}}$ which is required for the capture to occur, while the second one sets the lower limit of the energy integration to $\max[E_{\min}, E_{\text{cap}}]$.

Notice that, after the first upscattering of the DM particle χ , there are two possible situations that may arise depending on the lifetime of the heavier state χ' . If the lifetime of χ' is very short, it quickly decays back to χ along with other particle(s) which are much lighter and carry away most of the energy produced in the decay, so that no significant kinetic energy is imparted to χ . As a consequence, Eqs. (2.4) and (2.5) can be used to calculate the capture rate because a single scattering with $E > E_{\text{cap}}$ is sufficient to keep the χ particle gravitationally bound during the lifetime of the star, eventually driving it to the core of the celestial body after subsequent interactions with its nuclear targets. We will see that this is the situation which occurs in the types of DM models discussed in the next section. On the other hand, if the lifetime of χ' is large enough it eventually downscatters off a WD nuclear target back to a χ through an exothermic process that can in principle eject the outgoing DM particle to a nonbound orbit. In this case Eqs. (2.4) and (2.5) cannot be used to describe the capture process. However, if χ is much heavier than the target nucleus, the latter carries away most of the energy, leading to a situation where the DM particle does not have sufficient kinetic energy to escape from the star's gravitational potential and thus also in this case it is eventually captured [47]. Actually, in the present work we will be interested in the capture of TeV-scale DM particles, so they would be captured in the WD star after the first inelastic scattering with $E > E_{\text{cap}}$ even for χ' lifetimes longer than those discussed in Sec. III B.

The optically thin approximation holds when the scattering cross section [i.e., the integration of $\frac{d\sigma}{dE}$ over E in Eq. (2.5)] is small enough so that the effect of multiple scatterings can be neglected. If the cross section becomes very large, each DM particle that traverses the WD is captured and the capture rate saturates to its maximum value (known as the geometric limit), which is independent of the DM-nucleus interaction [30,34,44,49,50]:

$$C_{\text{geom}} = \pi R_*^2 \left(\frac{\rho_\chi}{m_\chi} \right) \int_0^\infty du \frac{f(u)}{u} w^2(R_*). \quad (2.7)$$

Finally, considering both regimes (i.e., optically thin and geometric regimes), the capture rate of DM in a WD star through inelastic scattering can be estimated as [31,44,49,51]

$$C_* = \min[C_{\text{opt-thin}}, C_{\text{geom}}]. \quad (2.8)$$

After being captured, the DM particles continue to scatter with the constituents of the WD and eventually thermalize and settle down to the WD interior where they can annihilate in pairs to produce various SM particles. The thermalization timescale is expected to be several orders of magnitude smaller than the typical age of the old and cold WDs (the types of which have been considered here) in the M4 globular cluster [34]. The evolution of the number of DM particles (N_χ) in the WD interior can be expressed as [34]

$$\frac{dN_\chi}{dt} = C_* - AN_\chi^2, \quad (2.9)$$

where A is the annihilation coefficient (which is proportional to the averaged annihilation cross section $\langle \sigma v \rangle$) and is related to the annihilation rate as

$$\Gamma_{\text{ann}} = \frac{1}{2}AN_\chi^2. \quad (2.10)$$

The primary SM particles injected by DM annihilation in a WD interior lead to further cascades and give rise to secondary particles which quickly thermalize in the medium of the star and thus end up in heating the star. Assuming that the total energy emitted in the DM annihilation process contributes to heat up the star, the resulting luminosity can be estimated as

$$L_\chi = 2m_\chi \Gamma_{\text{ann}}. \quad (2.11)$$

Note that, in reality, some percentage of the energy produced in DM annihilation inside the WD may be carried away by neutrinos which escape the star without heating it up. However, we have checked that, for the WDs considered here, neutrinos produced in the star core with energies above a GeV cannot come out from the star as their mean-free path, estimated using the number density of the WD constituents (obtained in [34] considering an improved analysis) and the interaction cross section of neutrinos with those constituents [52], is much smaller than the typical size of the WD star. The energetic neutrinos that cannot escape the star eventually thermalize in the star and are converted into electromagnetic radiation. In case of the annihilation of a TeV-scale DM (which is our present interest), the fraction of energy carried away by neutrinos with energies below 1 GeV (that are produced in the cascade of various primary annihilation states such as W^+W^- , ZZ , $b\bar{b}$) is less than 1–2% (estimated using [53]). Thus, we can assume that almost all of the energy produced in the annihilation contributes to the luminosity of the star and use Eq. (2.11) to calculate it. Notice that this implies that the ensuing bounds do not depend on assumptions on the primary SM states the DM particles annihilate to. This is at variance with capture in the Sun or the Earth

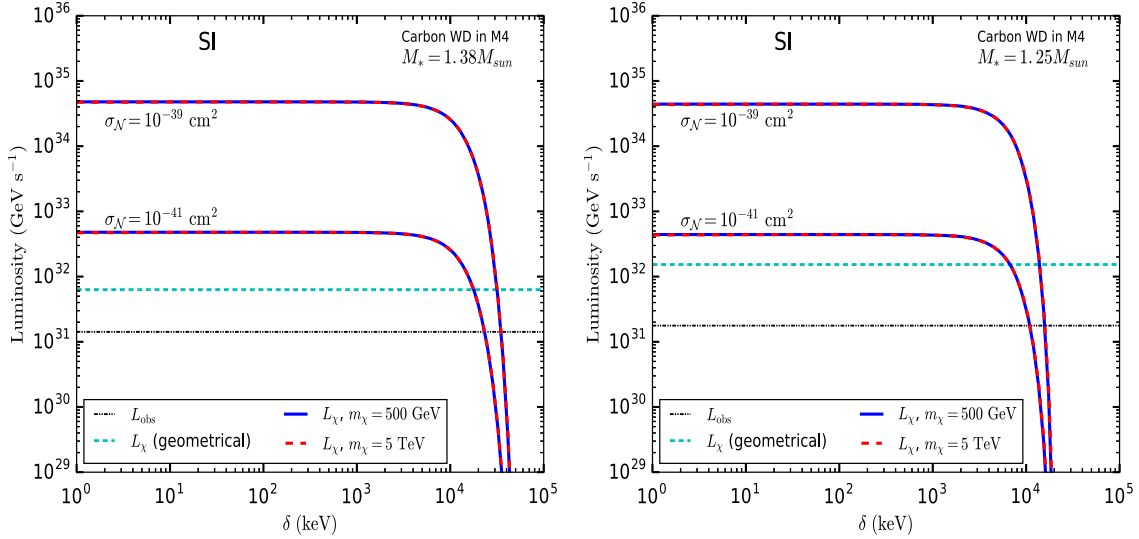


FIG. 1. DM-induced luminosities in both optically thin (blue and red lines) and geometric (cyan lines) limits as functions of δ , considering two benchmark carbon WDs in M4 with masses $M_* = 1.38 M_\odot$ (left panel) and $M_* = 1.25 M_\odot$ (right panel). The blue and the red lines are corresponding to the capture of 500-GeV and 5-TeV DM particles, respectively, assuming a spin-independent DM-nucleus interaction. In both panels the black horizontal lines indicate the luminosities (taken from [34]) that are observed for the considered WDs, while the cyan horizontal lines show the luminosities of the two benchmark WDs when DM capture is calculated in the geometric limit.

that may lead to a neutrino flux below the experimental energy threshold when the DM particles annihilate only to light states that are stopped before decaying.

The capture and annihilation processes inside the WD star equilibrate (so that $\frac{dN_\chi}{dt}$ becomes zero) over a timescale $\tau_{\text{eq}} = (C_* A)^{-1/2}$. A conservative estimate (following [31]) with the assumptions that $\langle \sigma v \rangle = \langle \sigma v \rangle_{\text{thermal}}$ and $C_* = C_{\text{geom}}$, the equilibrium timescale τ_{eq} (for DM particles of mass $m_\chi = 1$ TeV) turns out to be of the order of $\sim 10^{-6}$ Gyr for our benchmark WDs. This timescale is clearly several orders of magnitude lower than the typical ages of the old and faint WDs in M4, which are expected to be at least a few Gyrs [34]. Hence, one can in general assume equilibrium between the capture and annihilation processes inside these WDs in M4, and specifically in the model discussed in Sec. III. In that case the DM annihilation rate is $\Gamma_{\text{ann}} = C_*/2$ and the corresponding luminosity [given by Eq. (2.11)] becomes [30,34,41]

$$L_\chi = m_\chi C_*. \quad (2.12)$$

In Fig. 1, we show, as a function of the mass-splitting δ , the luminosities that are induced by the annihilation of inelastically captured DM particles in carbon WDs (located in M4) with masses and radii $M_* = 1.38 M_\odot$, $R_* \simeq 1.25 \times 10^3$ km (left panel) and $M_* = 1.25 M_\odot$, $R_* \simeq 3.29 \times 10^3$ km (right panel). The blue and the red lines in each panel represent the luminosities corresponding to the capture of DM with masses $m_\chi = 500$ GeV and 5 TeV, respectively, assuming a standard SI cross section with an

exponential (Helm) nuclear form factor [14,48] for the WIMP scattering events off carbon (^{12}C) in the optically thin limit [Eq. (2.4)]. In particular, two illustrative values of the DM-nucleon cross section $\sigma_{\mathcal{N}}$ have been used. The cyan horizontal lines in both panels of Fig. 1 show the luminosities obtained for the two benchmark WDs considering the capture of DM in the geometric limit [Eq. (2.7)]. Note that, since the capture rate falls as the inverse of m_χ in the geometric limit as well as in the optically thin limit (for $m_\chi \lesssim \mathcal{O}(10^5)$ GeV [34] and much larger than the target nucleus mass), the estimated luminosities in both regimes are independent of the DM mass.

The additional black lines shown in Fig. 1 represent the luminosities for the two considered WDs in M4 observed by the Hubble Space Telescope [54,55] and taken from [34]. These two WDs are among the faintest WDs observed in M4. Therefore, if the DM-predicted contribution to the total luminosity of these WDs is less than or at most equal to the observed ones, then there will be no contradiction between the DM prediction and the observations.

There are a few important points to notice in Fig. 1. The first one is that the DM luminosities calculated for the selected WDs in the optically thin limit are largely independent of δ up to a certain value of this parameter, beyond which the capture rates (hence the luminosities) start falling rapidly and ultimately go to zero when δ exceeds several tens of MeV. The second point is that the maximally achievable DM luminosity (i.e., the luminosity obtained in the geometric limit) for each WD is above the observed limit. Based on these two points, a comparison between the WD data and the DM luminosity [obtained

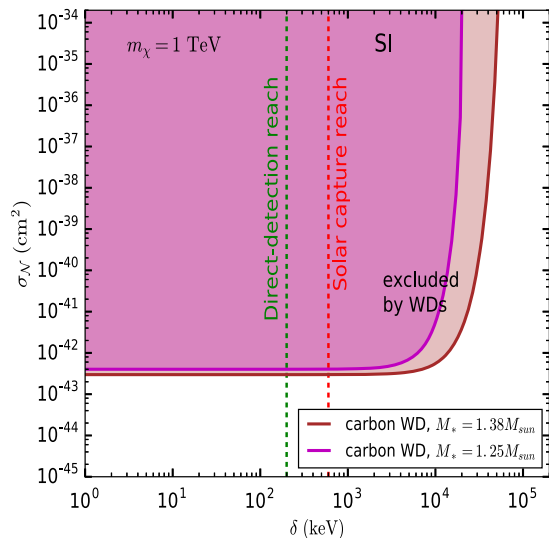


FIG. 2. Constraints in the $\sigma_{\mathcal{N}}$ vs δ plane (for a SI interaction) obtained using the observed luminosities for the two selected WDs in M4. The dashed green and red vertical lines show the maximum values of δ that can be probed in present direct-detection experiments and through solar neutrino searches, respectively.

using Eqs. (2.8) and (2.12)] enables one to constrain the DM interaction strength (for example, the DM-nucleon cross section $\sigma_{\mathcal{N}}$ in the case of a SI interaction) up to a maximum value of δ (a few tens of MeV for the WDs considered here), above which the DM luminosity goes below the observation. The maximum value of δ depends on the WD parameters and is larger for heavier WDs, since heavier and compact WDs have stronger gravitational potential which increases the kinematic upper limit on δ [see Eq. (2.1)]. Notice that the mass of the heaviest of our benchmark WDs almost saturates the Chandrasekhar limit $M_* \lesssim 1.4 M_{\odot}$ [56,57], and so in practice it kinematically saturates the best achievable bound on δ using WDs.

In order to illustrate the above discussion, we show in Fig. 2 the regions of the $\sigma_{\mathcal{N}}$ vs δ plane (for a SI interaction) that are excluded using the luminosity data of two selected faint WDs located in M4, assuming that they are made of carbon. The DM mass is taken to be $m_{\chi} = 1$ TeV, although, as mentioned earlier, for a sufficiently heavy DM (much heavier than the target nucleus) these constraints do not depend on m_{χ} . In the same figure the green and the red dashed lines indicate the maximum values of δ that can be probed in direct-detection experiments [27] and in solar neutrino searches [28], respectively. Figure 2 shows that WDs can improve the preexisting bounds on δ by more than one order of magnitude, ruling out δ up to a few tens of MeV for $\sigma_{\mathcal{N}} \gtrsim 3 \times 10^{-43}$ cm².

The constraints that we obtain here using the observations of faint and heavy WDs in M4 assume a spin-independent interaction between DM and the target nucleus. WDs are expected to be mostly composed of

spinless targets (^{12}C , ^{16}O or ^{20}Ne),¹ so that in order to derive constraints on spin-dependent (SD)-type interactions one needs to consider DM capture in other celestial objects such as the Sun. Notice that, as already pointed out, the reach on δ in the case of the Sun is considerably smaller (up to $\simeq 300$ keV for SD) [28,48].

Apart from WDs, one can also consider capture of DM particles in more compact objects such as neutron stars (NSs) [32,33,35,59], where the gravitational potential is so strong that the infalling DM particles are accelerated to quasirelativistic speeds. When such a high-speed DM particle collides with the NS constituents it can upscatter to the heavier state for a value of the inelastic splitting δ that can be as large as ~ 300 MeV [32,33]. The capture process of DM particles and their subsequent annihilation at the star core can heat a NS maximally up to a temperature T^{∞} (measured at a large distance from the NS) which is given by [32,60,61]

$$T^{\infty} \simeq 2300 \text{ K} \left(\frac{\rho_{\chi}}{0.4 \text{ GeV cm}^{-3}} \right)^{1/4} F \left(\frac{v_*}{230 \text{ km s}^{-1}} \right), \quad (2.13)$$

where ρ_{χ} is the DM density at the location of the NS, v_* is the velocity of the NS in the halo, and the function F is defined as

$$F(x) = \left[\frac{\text{Erf}(x)}{x \text{Erf}(1)} \right]^{1/4}. \quad (2.14)$$

Equation (2.13) corresponds to a temperature \simeq a few $\times 10^3$ K for nearby NSs. The observation of old NSs with such a low temperature is beyond the reach of existing telescopes but could be achievable by forthcoming infrared telescopes such as the James Webb Space Telescope (JWST), the Thirty Meter Telescope (TMT), and the European Extremely Large Telescope (E-ELT) [61–63].

III. CASE OF BIDOUBLET DM IN LEFT-RIGHT SYMMETRIC MODELS

The phenomenological discussion of Sec. II shows how WDs can provide bounds on the IDM scenario that are significantly stronger compared to those from DD. In this section we wish to illustrate the impact that such enhanced bounds can have on a specific IDM model, the fermion bidoublet extension of the LRSM.

The main motivation of the LRSM scenario is to explain one of the most puzzling features of the Standard Model, i.e., the observed maximal parity violation in its weak sector that forces to arrange the left-handed chiral components of fermions in $SU(2)$ electroweak doublets and their right-handed counterparts in singlets. In the LRSM

¹The abundance of targets with spin such as ^{13}C and ^{19}O in WDs is however subject to large uncertainties and strongly depends on the WD progenitor [58].

scenario the SM gauge group is enlarged in order to contain an $SU(2)_L$ and an $SU(2)_R$, so that the doublets of $SU(2)_L$ are singlets of $SU(2)_R$ and the doublets of $SU(2)_R$ are singlets of $SU(2)_L$. Interestingly, such scenarios can be easily extended by a multiplet that contains a dark matter candidate that is automatically stable [64,65] and whose mass is the only required additional free parameter. A detailed description of the LRSM scenario can be found in [66], and a discussion of the phenomenology of its DM extensions in [38]. In Sec. III A we will summarize the specific scenario where the LRSM model is extended with a fermion bidoublet that contains an IDM candidate, and in Sec. III B we apply the results of Sec. II B to constrain its parameter space. Moreover, in Sec. III C we discuss how the low-energy LRSM parameter space compatible with observation can be obtained when the LRSM model is embedded in a grand unified theory at high energy.

A. Model description

The gauge symmetry of LRSM is $SU(3) \times SU(2)_L \times SU(2)_R \times U(1)_{B-L}$, with B and L the baryon and lepton number. The representations under the different gauge groups of the fermions and scalars contained in the model are listed in Table II of the Appendix for both its minimal realization and for various extension that will be discussed in Sec. III C. In its minimal realization the LRSM preserves D parity, i.e., it is invariant by the interchange of any multiplet of $SU(2)_L$ into the corresponding $SU(2)_R$ multiplet. In particular, in one of the most popular variants of minimal LRSM the scalar sector contains an $SU(2)_L$ triplet T_L , an $SU(2)_R$ triplet T_R , and a scalar bidoublet Φ . The LR symmetry of the model is broken spontaneously down to the SM in two steps. First, the $SU(2)_R \times U(1)_{B-L}$ symmetry is broken spontaneously to $U(1)_Y$ at a high scale M_R by the vacuum expectation value (VEV) v_R of T_R , and the masses of the $SU(2)_R$ gauge bosons W_R and Z_R are generated. This breaks the parity invariance of the model and implies the relation $Y = T_R^3 + \frac{1}{2}(B-L)$ between the generator of $U(1)_Y$ and those of $U(1)_{B-L}$ and $SU(2)_R$. In particular, Z_R is a linear combination of W_R^3 (the gauge boson corresponding to the generator T_R^3) and B [the gauge boson for $U(1)_{B-L}$], while the orthogonal combination B_Y [the gauge boson corresponding to the remnant $U(1)_Y$ symmetry] remains massless at this stage. Notice that the breaking of $SU(2)_R \times U(1)_{B-L}$ also generates large Majorana masses for right-handed neutrinos. The second stage of symmetry breaking happens at the electroweak scale, when the scalar bidoublet Φ gets VEVs $v_1/\sqrt{2}$ and $v_2/\sqrt{2}$, and the intermediate $SU(2)_L \times U(1)_Y$ breaks down to the $U(1)_{em}$ symmetry, leading to the usual relation $Q = T_L^3 + Y$, so that $Q = T_L^3 + T_R^3 + \frac{1}{2}(B-L)$. This leads to the mass generation of all the known SM particles. Moreover, since Φ is a bidoublet, its VEVs generate mixings among left-handed and right-handed gauge

bosons. This also relates the gauge couplings in the following manner²:

$$\frac{1}{g_Y^2} = \frac{1}{g_R^2} + \frac{1}{g_{B-L}^2}, \quad (3.1)$$

$$\frac{1}{e^2} = \frac{1}{g_L^2} + \frac{1}{g_Y^2}, \quad (3.2)$$

where g_α is the gauge coupling of $U(1)_\alpha$ ($\alpha = B-L, Y$). The $SU(2)_{L(R)}$ gauge coupling is denoted by $g_{L(R)}$ while e is the gauge coupling of the residual $U(1)_{em}$. The three mixing angles among the neutral gauge bosons, i.e., θ_R (mixing between W_R^3 and B), θ_W (mixing between W_L^3 and B_Y , the Weinberg angle), and ϕ (mixing between Z_R and Z_L) are given by [38]

$$\begin{aligned} \theta_W &= \tan^{-1}\left(\frac{g_Y}{g_L}\right), & \theta_R &= \sin^{-1}\left(\frac{g_L \tan \theta_W}{g_R}\right), \\ \phi &\simeq \frac{1}{2} \tan^{-1}\left(-2 \cos \theta_W \cos \theta_R \frac{g_R M_{Z_L}^2}{g_L M_{Z_R}^2}\right), \end{aligned} \quad (3.3)$$

where

$$\begin{aligned} M_{Z_L}^2 &\simeq M_{Z_1}^2 = \frac{g_L^2}{4 \cos^2 \theta_W} v^2 = M_Z^2, \\ M_{Z_R}^2 &\simeq M_{Z_2}^2 = \frac{g_R^2}{\cos^2 \theta_R} v_R^2 + \frac{g_R^2}{4} \cos^2 \theta_R v^2. \end{aligned} \quad (3.4)$$

In Eq. (3.4) the mixing ϕ is neglected since $M_{Z_R} \gg M_{Z_L}$, Z is the Standard Model massive neutral gauge boson and $v = \sqrt{v_1^2 + v_2^2} = 246$ GeV. The expression of ϕ in Eq. (3.3) is valid in the phenomenological limit where $v_R \gg v_1, v_2$ and the VEV of T_L (v_L) $\rightarrow 0$. Similarly, when v_1 and v_2 are real the mixing angle between W_R^\pm and W_L^\pm is given, in the phenomenological limit, by [38]

$$\xi \simeq \frac{1}{2} \tan^{-1}\left(-4 \frac{g_R M_{W_L}^2 v_1 v_2}{g_L M_{W_R}^2 v^2}\right), \quad (3.5)$$

with

$$\begin{aligned} M_{W_L}^2 &\simeq M_{W_1}^2 = \frac{g_L^2}{4} v^2 = M_W^2, \\ M_{W_R}^2 &\simeq M_{W_2}^2 = \frac{1}{4} g_R^2 (v^2 + 2v_R^2), \end{aligned} \quad (3.6)$$

where M_W is the mass of the electroweak charged gauge boson of the Standard Model.

²When models are embedded into a grand unified theory, the normalization of g_R and g_{B-L} is that of Eqs. (A2) and (A3).

In the DM scenario that we wish to discuss, the LRSM is minimally extended by adding a self-conjugate fermionic bidoublet Ψ (with $\tilde{\Psi} \equiv -\sigma_2 \Psi^c \sigma_2 = \Psi$) having zero $B - L$ charge. In 2×2 matrix representation, the bidoublet Ψ can be written explicitly in terms of two Dirac field ψ^\pm and ψ^0 as [38]

$$\Psi = \begin{bmatrix} \psi^0 & \psi^+ \\ \psi^- & -(\psi^0)^c \end{bmatrix}. \quad (3.7)$$

The Lagrangian for Ψ is given by

$$\begin{aligned} \mathcal{L}_{\text{BD}} = & i\bar{\psi}^0 \partial \psi^0 + i\bar{\psi}^- \partial \psi^- + \frac{g_L}{2} (\bar{\psi}^0 \mathcal{W}_L^3 \psi^0 - \bar{\psi}^- \mathcal{W}_L^3 \psi^- + \sqrt{2} \bar{\psi}^0 \mathcal{W}_L^+ \psi^- + \sqrt{2} \bar{\psi}^- \mathcal{W}_L^- \psi^0) \\ & - \frac{g_R}{2} (\bar{\psi}^0 \mathcal{W}_R^3 \psi^0 + \bar{\psi}^- \mathcal{W}_R^3 \psi^- + \sqrt{2} \bar{\psi}^0 \mathcal{W}_R^- \psi^+ + \sqrt{2} \bar{\psi}^+ \mathcal{W}_R^+ \psi^0) - M_\Psi \bar{\psi}^0 \psi^0 - M_\Psi \bar{\psi}^- \psi^-. \end{aligned} \quad (3.10)$$

Although in Eq. (3.10) ψ^\pm and ψ^0 have the degenerate tree-level mass M_Ψ , a mass splitting

$$M_{\psi^\pm} - M_{\psi^0} \simeq Q \left(Q + \frac{2Y}{\cos \theta_W} \right) \Delta M, \quad (3.11)$$

with

$$\Delta M = \frac{g_L^2}{4\pi} M_{W_L} \sin^2 \frac{\theta_W}{2} \simeq 166 \text{ MeV},$$

is generated between the neutral and charged components by radiative corrections [64]. Due to such mass splitting the charged component ψ^\pm is unstable and decays into ψ^0 and π^\pm or a pair of light leptons on very short timescales $\mathcal{O}(10^{-11})$ s [38]. Notice that the specific representation of Ψ in Eq. (3.7) only allows the terms in Eq. (3.8), automatically preventing the decay of its lightest component ψ^0 , that is then a natural DM candidate.

Moreover, the Dirac nature of ψ^0 is only protected by the $SU(2)_L \times SU(2)_R$ symmetry, which is no longer a good symmetry after the bidoublet Φ acquires nonvanishing VEVs. Specifically, the $W_R^\pm - W_L^\pm$ mixing induces a transition at the one-loop level between ψ^0 and $(\psi^0)^c$ (with either W_1^\pm or W_2^\pm and ψ^\mp running in the loop) that generates a tiny ($\sim \mathcal{O}(\text{keV} - \text{MeV})$) off-diagonal Majorana mass term δM between ψ^0 and $(\psi^0)^c$ proportional to $\sin(2\xi)$ [38]. Consequently, the Dirac fermion splits into

$$\mathcal{L}_{\text{BD}} = \frac{1}{2} \text{Tr}[\bar{\Psi} i \not{D} \Psi] - \frac{1}{2} M_\Psi \text{Tr}[\bar{\Psi} \Psi], \quad (3.8)$$

with covariant derivative:

$$D_\mu \Psi = \partial_\mu \Psi - i \frac{g_L}{2} \sigma_a W_{L\mu}^a \Psi + i \frac{g_R}{2} \Psi \sigma_a W_{R\mu}^a. \quad (3.9)$$

Substituting the expressions of D_μ and Ψ in Eq. (3.8), the Lagrangian in terms of the component fields reads

two quasidegenerate Majorana fermions $\chi_{1,2}$ with opposite CP given by

$$\chi_{1,2} = \frac{1}{\sqrt{2}} (\psi^0 \mp (\psi^0)^c), \quad (3.12)$$

with

$$M_{\chi_{1,2}} = M_\Psi \mp \delta M, \quad (3.13)$$

providing in a natural way a specific realization of the IDM scenario that we discussed at the phenomenological level in Sec. II. The mass splitting between χ_1 and χ_2 is given by [38]

$$\delta = 2\delta M = \frac{g_L^2}{16\pi^2} \frac{g_R}{g_L} \sin(2\xi) M_\Psi [f(r_{W_1}) - f(r_{W_2})], \quad (3.14)$$

where $r_V = M_V/M_\Psi$ and the loop function $f(r_V)$ given by

$$f(r_V) = 2 \int_0^1 dx (1+x) \log [x^2 + (1-x)r_V^2]. \quad (3.15)$$

In particular, in the phenomenological analysis of Sec. III B we will assume $v_1 = v_2$ in order to maximize the splitting δ at fixed M_{W_2} and g_R [see Eq. (3.5)].

Finally, in terms of the physical states χ_1 and χ_2 Eq. (3.10) is given by

$$\begin{aligned} \mathcal{L}_{\text{BD}} = & \frac{i}{2} \bar{\chi}_1 \not{\partial} \chi_1 + \frac{i}{2} \bar{\chi}_2 \not{\partial} \chi_2 + i\bar{\psi}^- \not{\partial} \psi^- - \frac{M_{\chi_1}}{2} \bar{\chi}_1 \chi_1 - \frac{M_{\chi_2}}{2} \bar{\chi}_2 \chi_2 - M_{\psi^-} \bar{\psi}^- \psi^- \\ & + \frac{1}{2} \bar{\chi}_1 (g_L \mathcal{W}_L^3 - g_R \mathcal{W}_R^3) \chi_2 - \frac{1}{2} \bar{\psi}^- (g_L \mathcal{W}_L^3 + g_R \mathcal{W}_R^3) \psi^- \\ & + \left\{ \frac{1}{2} \bar{\chi}_1 (g_L \mathcal{W}_L^+ - g_R \mathcal{W}_R^+) \psi^- + \frac{1}{2} \bar{\chi}_2 (g_L \mathcal{W}_L^+ + g_R \mathcal{W}_R^+) \psi^- + \text{H.c.} \right\}, \end{aligned} \quad (3.16)$$

where $M_{\psi^-} \simeq M_\Psi + (1 + \sec \theta_W) \Delta M$ from Eq. (3.11).

Depending on the mass splitting δ the heavier bidoublet state χ_2 decays into the lighter state χ_1 via different channels, with the radiative decay $\chi_2 \rightarrow \chi_1 \gamma$ always kinematically allowed having a lifetime $\simeq 10^{-3} \text{ s} (\frac{1 \text{ MeV}}{\delta})^3$ [38] [such expression is valid when $M_\Psi \simeq \mathcal{O}(\text{TeV})$ and $\delta \ll M_\Psi$]. As a consequence, for the choice of parameters in the next section, by the present time all the χ_2 states have decayed and χ_1 is the DM candidate in our Universe.

B. Bounds from white dwarves on LRSM bidoublet dark matter

In this section we will identify χ and χ' with χ_1 and χ_2 . The process of inelastic scattering of χ against a WD nucleus occurs dominantly through the exchange of the light Z boson. The corresponding interaction Lagrangian (involving χ , χ' , and Z) can be written as

$$\mathcal{L}_{\chi\chi'Z} = g_\chi \bar{\chi} \not{Z} \chi', \quad (3.17)$$

where

$$g_\chi = \frac{1}{2} (g_L \cos \theta_W \cos \phi + g_R \sin \theta_W \sin \theta_R \cos \phi + g_R \cos \theta_R \sin \phi). \quad (3.18)$$

The coupling g_χ is obtained by expressing W_L^3 and W_R^3 in Eq. (3.16) in terms of the mass eigenstate Z , using the neutral gauge boson mixing matrix given in the appendix of [38]. Since the typical values of the momentum transfer in such a process are always much lower than M_Z , one can express the interaction of χ and χ' with SM quarks in terms of the following dimension-6 operators:

$$\begin{aligned} \mathcal{O}_{V,q}^{(6)} &= C_{V,q}^{(6)} (\bar{\chi} \gamma_\mu \chi') (\bar{q} \gamma^\mu q), \\ \mathcal{O}_{A,q}^{(6)} &= C_{A,q}^{(6)} (\bar{\chi} \gamma_\mu \chi') (\bar{q} \gamma^\mu \gamma_5 q), \end{aligned} \quad (3.19)$$

with

$$C_{V,q}^{(6)} = \frac{g_\chi g_L g_V^q}{M_Z^2 \cos \theta_W}, \quad C_{A,q}^{(6)} = \frac{g_\chi g_L g_A^q}{M_Z^2 \cos \theta_W}, \quad (3.20)$$

where g_V^q and g_A^q are defined in [67].

In the nonrelativistic limit the above interaction terms lead to a WIMP-nucleon interaction driven by the effective Hamiltonian:

$$\mathcal{H} = \sum_{N=p,n} (c_1^N \mathcal{O}_1^N + c_7^N \mathcal{O}_7^N + c_9^N \mathcal{O}_9^N), \quad (3.21)$$

(in the operator base of [68]), with p , n indicating proton and neutron. The Wilson coefficients c_1^N , c_7^N , and c_9^N in terms of the $C_{V,q}^{(6)}$ and $C_{A,q}^{(6)}$ quantities can be obtained for instance, from [69]. In particular, the effective operator \mathcal{O}_1

leads to a spin-independent WIMP-nucleus cross section proportional to the square of the atomic mass number of the target, while the \mathcal{O}_7 and \mathcal{O}_9 operators, which are velocity and momentum suppressed, vanish in the case of the spinless targets (^{12}C , ^{16}O or ^{20}Ne) that constitute the interior of a WD. Specifically, for the operator $\mathcal{O}_{V,q}^{(6)}$ one has $c_1^N = \sum_{q=u,d} C_{V,q}^{(6)} F_N^{(q)}$ with

$$F_p^{(u)} = 2, \quad F_p^{(d)} = 1, \quad (3.22)$$

$$F_n^{(u)} = 1, \quad F_n^{(d)} = 2, \quad (3.23)$$

while the WIMP-nucleon cross section σ_N introduced in Sec. II is given by $\sigma_N = (c_1^N)^2 \mu_{\chi N}^2 / \pi$. In order to evaluate the WD capture rate we have assumed that the WDs observed in M4 are made of carbon and we have calculated the differential cross section $\frac{d\sigma[\chi+N \rightarrow \chi'+N]}{dE}$ in Eq. (2.5) using the WimPyDD code [70,71].

In Fig. 3 the solid blue line and the dashed red line represent the result of the evaluation of the expected luminosity of Eq. (2.12) for the capture of LRSM bidoublet DM by WDs in the optically thin limit as a function of the mass-splitting parameter δ for DM masses $m_\chi = 500 \text{ GeV}$ and $m_\chi = 5 \text{ TeV}$, respectively, for $g_L = g_R$ and for the same carbon WDs of Fig. 1. In both plots the cyan and black dotted horizontal lines are the same of Fig. 1 and represent, respectively, the geometrical limit of the capture rate and the corresponding observed luminosities [34]. As expected, unless the capture process in the WD is kinematically forbidden the large WIMP-nucleus cross section implied by the nonvanishing hypercharge of the bidoublet saturates the geometrical capture upper bound and exceeds the observation. This is achieved for $\delta \gtrsim 40 \text{ MeV}$ (17 MeV) for $M_* = 1.38 M_\odot$ ($M_* = 1.25 M_\odot$).

Notice that, as described in Sec. III A, the heavier bidoublet state χ' decays to the DM state χ within a timescale that is extremely small compared to the typical age of the WDs in M4, expected to be a few Gyrs. In such a case, the expressions of the capture rate given in Sec. II B apply, and the final population of DM particles in the WD core consists of only χ . The pair annihilation of these particles, which is driven by t -channel processes, injects electroweak gauge bosons whose cascade products thermalize in the WD medium and heat up the star.

As already pointed out in Sec. II, the bound from WDs is much more constraining than that expected from direct detection and from solar neutrino searches. The impact from such bound on the m_χ - M_{W_2} parameter space of the LRSM bidoublet dark matter is shown in Fig. 4 for $g_R = g_L$, which represents the most commonly used value in phenomenological and experimental analyses. In the upper-left corner the green-shaded area shows the part of parameter space excluded by direct detection, which can

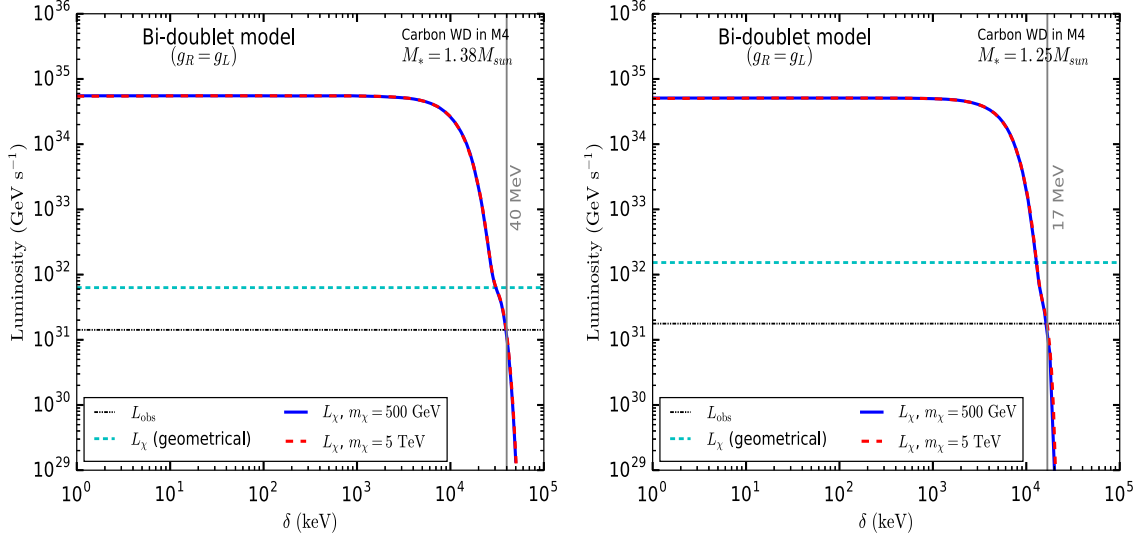


FIG. 3. Bidoublet DM-induced luminosities in optically thin (solid blue and red dashed lines) and geometric (horizontal cyan lines) limits as functions of the mass splitting δ , considering two benchmark carbon WDs in M4 with masses $M_* = 1.38 M_\odot$ (left panel) and $M_* = 1.25 M_\odot$ (right panel). The solid blue line and the red dashed line correspond to the capture of 500-GeV and 5-TeV DM particles, respectively. The black dotted lines in both panels represent the luminosities observed for the considered WDs [34]. The vertical gray lines indicate the maximum values of δ that are possible to probe for these WDs.

probe $\delta \lesssim 200$ keV [27], while the red-shaded one the part of parameter space excluded by the solar neutrino searches, which can probe $\delta \lesssim 600$ keV [28]. On the other hand, the pink-shaded region is excluded by the nonobservation of

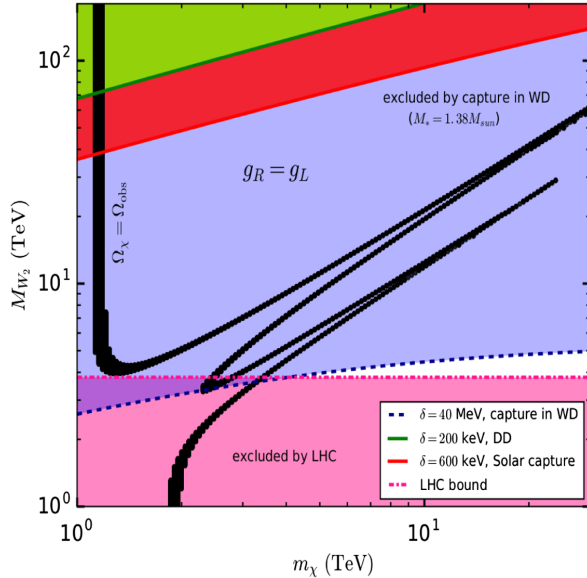


FIG. 4. The region of the bidoublet parameter space (spanned by M_{W_2} and the bidoublet DM mass m_χ) that is excluded by the observation of the faintest and heaviest ($M_* = 1.38 M_\odot$) WD (assuming it is made of carbon) in M4 is shown by the blue-shaded area, considering $g_R = g_L$. The pink, green, and red shaded areas correspond to the regions excluded by LHC search, DD experiments, and solar neutrino search, respectively. The black band consists of parameter points where the calculated thermal relic density is in the observed range.

the W_2 boson at the LHC ($M_{W_2} < 3.8$ TeV [72]), and the black band represents the region where the thermal relic density is in the observed range ($0.11 \leq \Omega h^2 \leq 0.13$). As shown in such figure, when only the direct detection, solar neutrino searches, and the LHC bounds are considered (as done in the literature so far [38]) the LRSM bidoublet is a viable DM candidate in a wide range of masses, 1.1 TeV $\lesssim m_\chi \lesssim 30$ TeV and for $g_R = g_L$. However, when the bound from WD is considered this changes considerably: in Fig. 4 the blue-shaded area, which lies above the dashed blue line for $\delta = 40$ MeV, represents the parameter space excluded by WDs. Indeed, for $g_R = g_L$ the full cosmologically viable parameter space now lies in such region and is ruled out. As pointed out below Eq. (3.14) in our calculation we have maximized δ at fixed m_χ , g_R , and M_{W_2} in terms of the other parameters of the model. As a consequence, for other choices of such parameters the M_{W_2} values excluded by WDs would be even lower, so that the excluded region of Fig. 4 should be considered as a conservative one.

In order to evade the WD constraint one needs to increase further the value of the mass-splitting parameter δ at fixed m_χ and M_{W_2} . As shown in Eq. (3.14), the only way to achieve this within the available parameter space is to choose $g_R > g_L$. This is done in Fig. 5, where $g_R/g_L = 1.2$ in the left-hand plot, and $g_R/g_L = 1.8$ in the right-hand plot. Indeed, now in both cases some cosmologically viable parameter space is recovered. In particular, for $g_R/g_L = 1.2$ this requires $M_{W_2} \lesssim 6$ TeV, and 3.5 TeV $\lesssim m_\chi \lesssim 5$ TeV, while for $g_R/g_L = 1.8$ $M_{W_2} \lesssim 12$ TeV and two bidoublet allowed mass ranges are found: 1.2 TeV $\lesssim m_\chi \lesssim 3$ TeV and 5 TeV $\lesssim m_\chi \lesssim 10$ TeV. In Sec. III C we will discuss how $g_R/g_L > 1$ can be achieved at low energy when the

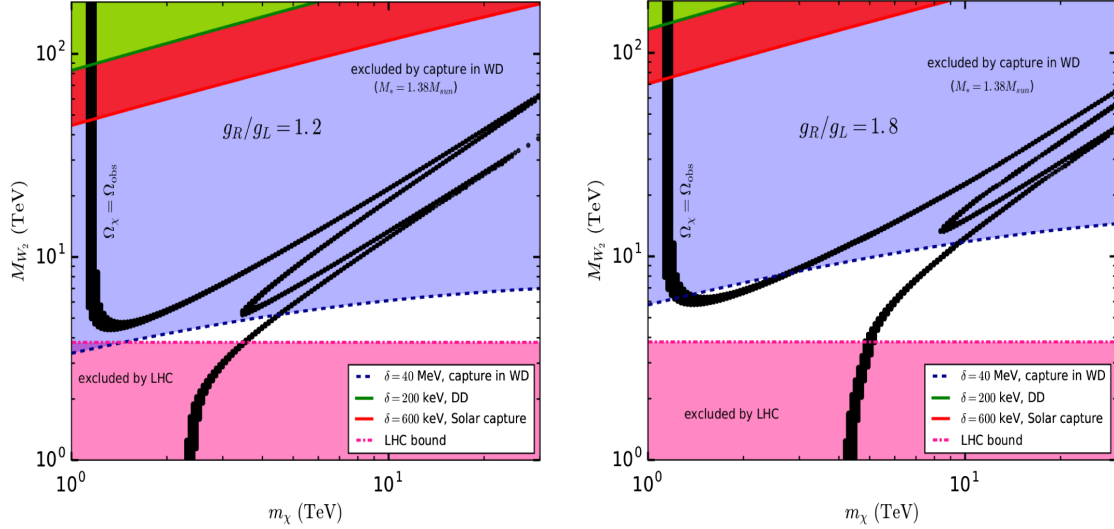


FIG. 5. Same as Fig. 4, but considering scenarios with $g_R/g_L = 1.2$ (left panel) and $g_R/g_L = 1.8$ (right panel).

LRSMD model is embedded at high scale in a grand unified theory, and provide an explicit example with $g_R/g_L \simeq 1.2$. On the other hand we consider $g_R/g_L = 1.8$ a reasonable estimation of the maximal allowed value of such ratio since it roughly coincides to the perturbative upper bound discussed in [73].³

For the calculation of the bidoublet relic abundance in Figs. 4 and 5 we have modified the FeynRules [74] implementation of the LRSMD model of Ref. [75] in order to allow $g_R \neq g_L$, and used it to produce a CalcHEP [76] output file, which we have then modified implementing the Lagrangian of Eq. (3.10).⁴ Finally, we have used such modified CalcHEP file in MicrOMEGAs [77].

C. Consequences at high scale

The implementation of the bound from WDs in the phenomenological analysis of Sec. III B singles out a relatively well-defined parameter space in order for the LRSMD bidoublet scenario to provide a viable DM candidate, characterized by a low mass for the W_2 boson ($M_{W_2} \lesssim 10$ TeV) and $g_R > g_L$. In this section we wish to discuss whether such parameter space can be obtained, and how naturally, when the LRSMD model is embedded in a grand unified theory, which represents its most popular ultraviolet completion.

The LRSMD scenario naturally arises in GUT. Indeed, many scenarios have been discussed in the literature

[78–83], where the LR group $SU(2)_L \times SU(2)_R$ is embedded into a GUT $SO(10)$. Specific examples include: (i) $SO(10) \supset SU(2)_L \times SU(2)_R \times SU(4)_C \times D$; (ii) $SO(10) \supset SU(2)_L \times SU(2)_R \times SU(4)_C$; (iii) $SO(10) \supset \text{LRSMD} \equiv SU(2)_L \times SU(2)_R \times SU(3)_C \times U(1)_{B-L} \times D$, and (iv) $SO(10) \supset \text{LRSMD}\emptyset \equiv SU(2)_L \times SU(2)_R \times SU(3)_C \times U(1)_{B-L}$. Here D stands for the parity symmetry that leaves the theory invariant by the interchange of any multiplet of $SU(2)_L$ into the corresponding $SU(2)_R$ multiplet. The low-energy scenario discussed in Secs. III A and III B corresponds to either LRSMD or LRSMD \emptyset extended with the DM bidoublet Ψ (LRSMD + Ψ and LRSMD \emptyset + Ψ in the following).

In the analysis of Sec. III B we have used WDs to constrain the bidoublet LRSMD parameter space at the phenomenological level, i.e., taking the low-energy parameters of the model introduced in Sec. III A ($M_{\chi_1} = m_{\chi}$, M_{W_2} , g_R , and v_1/v_2) as independent without assuming any specific ultraviolet completion. In a GUT theory context such parameters are expected to be correlated. In the literature, most often the so-called *minimal* version of the LRSMD assumes D parity. However, in the following we will consider both cases, conserved D parity and broken D parity.

The most important appeal of GUT is the unification of gauge couplings at high energy, which comes together with the salient prediction of proton decay. Therefore, once the embedding of the LR models in a GUT framework comes into play we need to pay attention to the GUT scale and to the proton decay rate. In particular, in some of its realizations LRSMD models embedded in $SO(10)$ typically achieve a unification scale around 10^{15} GeV, which leads to proton decay rates incompatible with the experimental constraints. Specifically, for the minimal particle content of Table II and the embedding (i) the breaking of the $SU(2)_R$

³See Fig. 7 of [73]. However, at variance with Fig. 5, in the discussion of Ref. [73] $g_R/g_L = 1.8$ is correlated to a high M_{W_2} mass, $M_{W_2} \gtrsim 90$ TeV.

⁴The relic abundance can be directly calculated in terms of the Ψ^0 and Ψ^\pm Dirac fermions of the bidoublet of Eq. (3.7), since in the early Universe the effect of the mass splitting is negligible in the calculation of the annihilation cross section.

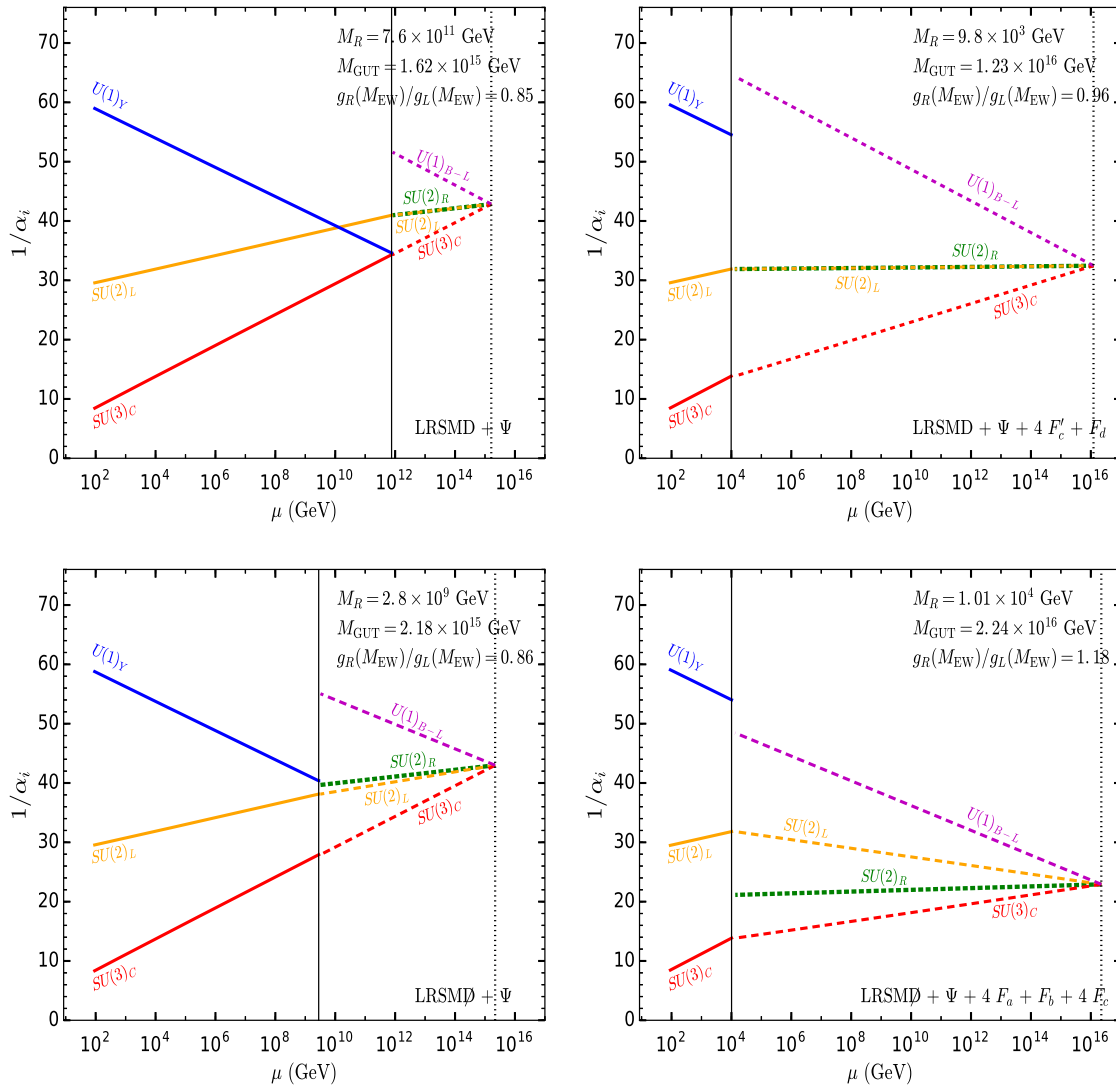


FIG. 6. Running of the inverse of the gauge couplings α_i of the LRSM models we consider. Top panels: D -parity conserving scenarios. Top left: LRSMD + Ψ , minimal model plus dark matter bidoublet. Top right: LRSMD + $\Psi + 4F'_c + F_d$. Bottom panels: scenarios with broken D parity. Bottom left: LRSMD + Ψ , minimal model plus dark matter bidoublet. Bottom right: LRSMD + $\Psi + 4F_a + F_b + 4F_c$. The definition of the fermions F_i is given in Table II. The value of M_R (M_{GUT}) corresponding to each case is indicated by the black solid (dotted) line.

is achieved at around $M_R \approx 10^{13}$ GeV and the GUT scale is $M_{\text{GUT}} \approx 10^{15}$ GeV. On the other hand, for (ii) M_R is around 10^{11} GeV, while $M_{\text{GUT}} \approx 10^{16}$ GeV. For (iii) LRSMD, $M_R \approx 10^{10}$ GeV, while the unification scale is achieved around $M_{\text{GUT}} \approx 10^{15}$ GeV. Finally, for (iv) LRSMD, $M_R \approx 10^9$ GeV and $M_{\text{GUT}} \approx 10^{16}$ GeV [84].⁵

These basic scenarios hence do not offer an explanation of why $v_R \approx M_{W_2} \lesssim 10^4$ GeV, as emerging from Fig. 4 (notice that, depending on the specific mechanism of

symmetry breaking, it is natural to expect that v_R also determines the WIMP mass m_χ).

Extending the LRSMD model by adding only the DM bidoublet fermion (the LRSMD + Ψ case) actually slightly increases the value $M_R \simeq v_R$ of the scale at which $SU(2)_R$ is broken and increases the proton decay (PD) lifetime (see Table I).⁶ So, although adding Ψ to the model can increase the PD lifetime (albeit not enough in most cases), it is of no help to reduce M_R . This case is shown in the top-left plot of Fig. 6, where the running of the coupling constants is

⁵For the exact values of M_R and M_{GUT} in each case check the original references and the updates of [85,86].

⁶It is well known that in nonsupersymmetric theories the dominant decay channel is $p \rightarrow \pi^0 e^+$. For specific formulas see for example Appendix D of [85] and Secs. 3 and 4.2 of [87].

TABLE I. Proton decay lifetime $\tau(p \rightarrow \pi^0 e^+)[\text{yrs}]$. The 1σ errors are extracted from a chi square with the observables at the electroweak scale.

Model predictions	
LRSMD	$(1.3 \pm 0.9) \times 10^{32}$
LRSMD + Ψ	$(2.9 \pm 1.9) \times 10^{32}$
LRSMD + $\Psi + 4 F'_c + F_d$	$(5.4 \pm 3.7) \times 10^{36}$
LRSMD \cancel{D}	$(3.8 \pm 2.5) \times 10^{36}$
LRSMD \cancel{D} + Ψ	$(7.6 \pm 5.2) \times 10^{32}$
LRSMD \cancel{D} + $\Psi + 4 F_a + F_b + 4 F_c$	$(2.0 \pm 1.3) \times 10^{37}$
Experimental bounds/discovery	
Current bound: 1.6×10^{34} at 95% CL [89,90]	Projected discovery: 6.3×10^{34} [91]
Projected bound: 7.8×10^{34} 90% CL [91]	

plotted as a function of the energy scale μ . As a consequence, in order to lower M_R one needs to add extra matter (in particular, all the additional degrees of freedom discussed in the following examples are listed in Table II). In [88] it was found that adding color multiplets is key to lower M_R down to 10^5 or 10^4 GeV. Notice that such additional high-scale degrees of freedom do not affect the phenomenology discussed in Sec. III B. In the top-right plot of Fig. 6 we show a specific example of this, where the MLRSM model is extended to include, besides the DM fermion bidoublet Ψ , four fermions F'_c , which are triplets under $SU(3)_C$ and singlets under all other interactions except for the D -parity charge, and one fermion F_d , which is a bidoublet under $SU(2)_R$ and $SU(2)_L$ and can have a nonzero D -parity charge. We can see that now the scale M_R is lowered. However, the ratio g_R/g_L is still smaller than one at the electroweak scale $M_{\text{EW}} \simeq 10^2$ GeV.

The feature $g_R(M_{\text{EW}})/g_L(M_{\text{EW}}) < 1$ (that for simplicity will be just indicated as g_R/g_L in the discussion below) is always present in D -parity conserving models since the running of g_R and g_L only splits below M_R , where g_R practically stops evolving while the value of g_L gets larger as the energy scale is decreased (notice that in Fig. 6 inverse couplings are plotted). So, the only way to obtain $g_R/g_L > 1$ is to break D parity at high scale, i.e., to split the running of g_R and g_L for $M_R < \mu < M_{\text{GUT}}$, so that $g_R > g_L$ already at M_R . This can be achieved in different ways which are anomaly free [88]. The most straightforward is by simply omitting the left-handed triplet T_L [73] (also this does not affect the phenomenology). This case, indicated by LRSMD \cancel{D} + Ψ , is shown in the bottom-left plot of Fig. 6. Since the scale M_R is lower than for the LRSMD + Ψ case the ratio g_R/g_L turns out to be slightly bigger but nevertheless less than 1 (notice also that in this case PD is not

TABLE II. The matter content of the minimal left-right symmetric model and its extensions discussed in Sec. III C. The LRSM with broken D parity does not contain T_L , while the one with D -parity conservation does.

Minimal left-right symmetric model		
Matter	Generations	$SU(2)_L \times SU(2)_R \times U(1)_{B-L} \times SU(3)_C$
Fermions		
L_L	3	$(\mathbf{2}, \mathbf{1}, -1, \mathbf{1})$
L_R	3	$(\mathbf{1}, \mathbf{2}, -1, \mathbf{1})$
Q_L	3	$(\mathbf{2}, \mathbf{1}, +\frac{1}{3}, \mathbf{3})$
Q_R	3	$(\mathbf{1}, \mathbf{2}, +\frac{1}{3}, \mathbf{3})$
Scalars		
Φ	1	$(\mathbf{2}, \bar{\mathbf{2}}, 0, \mathbf{1})$
T_R	1	$(\mathbf{1}, \mathbf{3}, +2, \mathbf{1})$
T_L	1	$(\mathbf{3}, \mathbf{1}, +2, \mathbf{1})$
DM Candidates		
Fermion		
Ψ	1	$(\mathbf{2}, \mathbf{2}, 0, \mathbf{1})$
Additional matter for conserving D parity		
Fermions		
F'_c	4	$(\mathbf{1}, \mathbf{1}, 0\mathbf{3})_L \oplus (\mathbf{1}, \mathbf{1}, 0, \mathbf{3})_R$
F_d	1	$(\mathbf{2}, \mathbf{2}, 0\mathbf{1})_L \oplus (\mathbf{2}, \mathbf{2}, 0, \mathbf{1})_R$
Additional matter for \cancel{D} parity		
Fermions		
F_a	4	$(\mathbf{2}, \mathbf{1}, 0\mathbf{3})$
F_b	1	$(\mathbf{1}, \mathbf{2}, 0, \mathbf{3})$
F_c	4	$(\mathbf{1}, \mathbf{1}, 0, \mathbf{3})$

consistent with observation). For this reason, in the final example shown in the bottom-right plot of Fig. 6 we add more fermions transforming under $SU(2)_L$ only than under $SU(2)_R$, so that the slope of g_L with respect to the energy scale μ gets steeper compared to g_R . In such scenario, indicated with LRSMD \cancel{D} + $\Psi + 4 F_a + F_b + 4 F_c$, we add four fermions F_a which are doublets of $SU(2)_L$, triplets of $SU(3)_C$, and singlets of the other groups, one fermion F_b , which is a doublet of $SU(2)_R$, triplet of $SU(3)_C$, and singlet of the other groups, and four fermions F_c which are triplets of $SU(3)_C$ and singlets under the rest of the groups (see Table II). Indeed, now $g_R/g_L \simeq 1.2$ is achieved. This case then provides an example where the value of M_R can be explained to be around 10^4 GeV without any fine-tuning, $M_{\text{GUT}} \gtrsim 10^{16}$ GeV so that the PD lifetime can be acceptable (see Table I), and $g_R/g_L > 1$.

The values of the ratio g_R/g_L are provided for all the models discussed above in Fig. 6. To get the plots of Fig. 6 we obtained the corresponding beta functions, given in Table III, using the code `pyr@te` [92] and used them in a private Runge-Kutta code.

TABLE III. Beta functions of the models we consider. The order of the indices is $i = L, R, BL, 3$.

Model	$b_i^{(1)}$	$b_{ij}^{(2)}$
LRSMD + Ψ	$\begin{pmatrix} -5/3 \\ -5/3 \\ 7 \\ -7 \end{pmatrix}$	$\begin{pmatrix} 209/6 & 9/2 & 27/2 & 12 \\ 9/2 & 209/6 & 27/2 & 12 \\ 81/2 & 81/2 & 115/2 & 4 \\ 9/2 & 9/2 & 1/2 & -26 \end{pmatrix}$
LRSMD + $\Psi + 4F'_c + F_d$	$\begin{pmatrix} -1/3 \\ -1/3 \\ 7 \\ -13/3 \end{pmatrix}$	$\begin{pmatrix} 307/6 & 15/2 & 27/2 & 12 \\ 15/2 & 307/6 & 27/2 & 12 \\ 81/2 & 81/2 & 115/3 & 2 \\ 9/2 & 9/2 & 1/2 & 74/3 \end{pmatrix}$
LRSMD + Ψ	$\begin{pmatrix} -7/3 \\ -5/3 \\ 11/2 \\ -7 \end{pmatrix}$	$\begin{pmatrix} 97/6 & 9/2 & 3/2 & 12 \\ 9/2 & 209/6 & 27/2 & 12 \\ 9/2 & 81/2 & 61/2 & 4 \\ 9/2 & 9/2 & 1/2 & -26 \end{pmatrix}$
LRSMD + $\Psi + 4F_a + F_b + 4F_c$	$\begin{pmatrix} 5/3 \\ -2/3 \\ 11/2 \\ -7/3 \end{pmatrix}$	$\begin{pmatrix} 391/6 & 9/2 & 3/2 & 28 \\ 9/2 & 565/12 & 27/2 & 16 \\ 9/2 & 81/2 & 61/3 & -1 \\ 21/2 & 6 & 1/2 & 188/3 \end{pmatrix}$

IV. CONCLUSIONS

Models of structure formation suggest that the inner part of globular clusters may have a DM density that largely exceeds that estimated in the solar neighborhood. Assuming this is so and that the DM is a WIMP particle, compact stars such as white dwarves can capture WIMPs through a process similar to that studied in the case of the Sun or the Earth, leading to an increase of the star luminosity through their annihilation process. As a consequence the issue of the amount of DM in globular clusters, and specifically in M4, has drawn increasing interest in the literature [29,34,41]. We have shown that if the WIMP interacts with the nuclear targets within the WD through inelastic scattering, the data on low-temperature large-mass WDs in the Messier 4 globular cluster can lead to a constraint on the mass splitting $\delta \lesssim$ few tens of MeV that largely exceeds that ensuing from direct detection in terrestrial underground experiments, $\delta \lesssim 200$ keV, and from solar neutrino searches, $\delta \lesssim 600$ keV, for a generic WIMP with a spin-independent cross section off nucleons larger than \simeq a few $\times 10^{-43}$ cm², assuming conservatively that the WD is entirely composed of carbon.

We have applied such improved constraint to the specific DM scenario of a self-conjugate bidoublet in the LRSM, where the standard $SU(2)_L$ group with coupling g_L is extended by an additional $SU(2)_R$ with coupling g_R in order to explain maximal parity violation in weak interactions. The ensuing bounds significantly reduce the cosmologically viable parameter space of such scenario, in particular requiring $g_R > g_L$. For instance, for $g_R/g_L = 1.8$ we have found the two viable mass ranges for the bidoublet DM candidate, $1.2 \text{ TeV} \lesssim m_\chi \lesssim 3 \text{ TeV}$ and $5 \text{ TeV} \lesssim m_\chi \lesssim 10 \text{ TeV}$, when the charged $SU(2)_R$ gauge boson mass M_{W_2} is less than $\simeq 12$ TeV.

In Sec. III C we have provided a short discussion on how such phenomenological parameter space at low energy can be achieved when the LRSM model is embedded at high scale in a GUT, showing that in the minimal scenario of LRSM + DM bidoublet one naturally gets $M_{W_2}, m_\chi \gtrsim 10^{10}$ GeV, and $g_R < g_L$, with a GUT scale $M_{\text{GUT}} \simeq 10^{15}$ GeV incompatible with proton decay bounds. As a consequence, one needs to extend the ultraviolet completion of the LRSM model with additional multiplets besides the DM bidoublet in order for the latter to explain the DM in the Universe in agreement with the WD bounds discussed in Sec. III B. Specifically, we found that adding color triplets that are singlets under all other groups and carry zero B-L charges can naturally yield $M_{W_2}, m_\chi \lesssim 10$ TeV. On the other hand, the only way to obtain $g_R > g_L$ is to split the running of g_R and g_L by assuming that D parity is broken at high scale, i.e., by introducing an asymmetry between the multiplets of $SU(2)_L$ and $SU(2)_R$. We provided a specific example of such scenario in Fig. 6, with the particle content of Table II.

We conclude by reminding that the amount of DM in M4 is still controversial. Our analyses motivate further studies to settle this issue. Moreover, at the end of Sec. II B we pointed out that the WDs bounds discussed in the present paper could be extended using more dense stellar object such as neutron stars, probing values of the inelastic splitting δ as large as ~ 300 MeV. In particular, a future observation of neutron stars with temperatures $T \lesssim$ a few thousand kelvin would rule out the full parameter space of LRSM bidoublet DM.

ACKNOWLEDGMENTS

We thank Alexander Pukhov and Julian Heeck for useful discussions. We thank Lohan Sartore for helping us with

running `pyr@te`. This research was supported by the National Research Foundation of Korea (NRF) funded by the Ministry of Education through the Center for Quantum Space Time (CQUeST) with Grant No. 2020R1A6A1A03047877 and by the Ministry of Science and ICT with Grant No. 2021R1F1A1057119. L. V.-S. acknowledges the KIAS warm hospitality and stimulating environment in these challenging times.

APPENDIX: ULTRAVIOLET COMPLETIONS OF THE LRSM MODEL AND BETA FUNCTIONS

The beta functions of the gauge couplings at two loops determine to a pretty good accuracy the unification and breaking of the $SU(2)_R$ scales. At two loops, the gauge couplings are only affected by their own running and the running of the top Yukawa coupling and hence one can consider the running of these quantities, without making any assumptions about the running of all of the other parameters of the theory. Obviously, for a specific model one must perform a complete running of all the parameters, but M_R and M_{GUT} can be determined to a great accuracy. For the beta functions of the gauge couplings of the models we present, we adopt the convention

$$\frac{dg_i}{dt} = \frac{b_i}{16\pi^2} g_i^3 + \frac{g_i^3}{(16\pi^2)^2} \left[\sum_{j=1}^{j=3} b_{ij} g_j^2 - c_i y_i^2 \right], \quad (\text{A1})$$

where g_i are the gauge couplings of each i factor and y_i is the gauge couplings of top Yukawa coupling. The coefficients b_i , b_{ij} , and c_i are determined by group invariants and the matter content of the theory. The beta functions of the basic LR symmetric model are well known for the D -parity conserving case, e.g., at one loop [88] and at two loops [86,93], and can be easily checked with `pyr@te` [92]. For the one-loop beta functions of other models we use [88] and `pyr@te` [92] for cross checking and two-loop computations. The coefficients of the beta functions for all the models we present in Sec. III C are given in Table III. Due to GUT embedding the matching of the LR gauge couplings to the SM gauge couplings is given by

$$\begin{aligned} g_{B-L}^{LR}(M_R) &= z \sqrt{\left(\frac{2}{5z^2} + \frac{3}{5} \right)} g_1^{\text{SM}}(M_R), \\ g_L^{LR}(M_R) &= g_2^{\text{SM}}(M_R), \\ g_C^{LR}(M_R) &= g_3^{\text{SM}}(M_R), \end{aligned} \quad (\text{A2})$$

where

$$g_{B-L}^{LR}(M_R) = z g_R^{LR}(M_R). \quad (\text{A3})$$

Here, z is a real number of $\mathcal{O}(1)$ that is determined through the constraint of unification at M_{GUT} . The gauge couplings obtained in the plots in Fig. 6 correspond to the last running

of the program that looks for convergence of the up and down running of the gauge couplings with the boundary conditions at M_{EW} and gauge unification at M_{GUT} . The matching to the SM model is given by

$$\frac{1}{g_1^2(M_R)} = \frac{2}{5} \frac{1}{g_{B-L}^2(M_R)} + \frac{3}{5} \frac{1}{g_R^2(M_R)}, \quad (\text{A4})$$

$$g_2^{\text{SM}}(M_R) = g_L^{LR}(M_R), \quad (\text{A5})$$

$$g_3^{\text{SM}}(M_R) = g_3^{LR}(M_R). \quad (\text{A6})$$

We have used the input parameters given in Table 1 of [87].

In order to understand why the addition of color triplets can drastically lower the scale M_R , we consider the one-loop beta function coefficients of the minimal LRSM models (both D conserving and D breaking). These coefficients can be written as

$$\begin{aligned} \begin{pmatrix} b_L \\ b_R \\ b_{B-L} \\ b_3 \end{pmatrix} &= \begin{pmatrix} -6 \\ -6 \\ 4/3 \\ -29/3 \end{pmatrix} + N_{HBD} \begin{pmatrix} 1/3 \\ 1/3 \\ 0 \\ 0 \end{pmatrix} \\ &+ N_{HT_L} \begin{pmatrix} 0 \\ 2/3 \\ 3 \\ 0 \end{pmatrix} + N_{HT_R} \begin{pmatrix} 2/3 \\ 0 \\ 3 \\ 0 \end{pmatrix}, \end{aligned} \quad (\text{A7})$$

where N_{HBD} is the number of Higgs bidoublets, N_{HT_L} and N_{HT_R} are the number of Higgs left triplets and right triplets, respectively. The first term on the right-hand side of Eq. (A7) corresponds to the one-loop beta functions from gauge interactions and the three families of fermions of the LRSM. In the D -parity conserving case both the left- and right-handed triplets T_L and T_R are present and $b_L = b_R = -5/3$. On the other hand, when only T_R is included D parity is broken and $b_R > b_L = -7/2$.

In order to obtain a phenomenologically viable scenario at low energy one needs to push the M_R and M_{GUT} scales further apart compared to the minimal cases LRSM + Ψ and LRSM + Ψ . In Fig. 6 $b_i < 0$ implies a positive slope for $1/\alpha_i$. Indeed, the addition of color triplets makes b_3 less negative, flattening the running of $1/\alpha_3$ and shifting M_{GUT} to higher scales and M_R to lower scales. However, adding only color triplets is not enough because multiplets of all the other groups are required in order to ensure that g_L and g_R unify at high scale. In particular, in order to increase the g_R/g_L ratio more multiplets of $SU(2)_L$ than of $SU(2)_R$ are needed in order to keep the one-loop beta function b_R as negative as possible so that $g_R(M_R) > g_L(M_R)$ already at the scale M_R (moreover, to overcome the running of g_L the hierarchy between the two couplings needs to be strong enough).

- [1] M. Schumann, Direct detection of WIMP dark matter: Concepts and status, *J. Phys. G* **46**, 103003 (2019).
- [2] R. K. Leane *et al.*, Snowmass2021 cosmic frontier white paper: Puzzling excesses in dark matter searches and how to resolve them, arXiv:2203.06859.
- [3] G. Arcadi, M. Dutra, P. Ghosh, M. Lindner, Y. Mambrini, M. Pierre, S. Profumo, and F. S. Queiroz, The waning of the WIMP? A review of models, searches, and constraints, *Eur. Phys. J. C* **78**, 203 (2018).
- [4] A. Boveia and C. Doglioni, Dark matter searches at colliders, *Annu. Rev. Nucl. Part. Sci.* **68**, 429 (2018).
- [5] S. Giagu, WIMP dark matter searches with the ATLAS detector at the LHC, *Front. Phys.* **7**, 75 (2019).
- [6] J. M. Gaskins, A review of indirect searches for particle dark matter, *Contemp. Phys.* **57**, 496 (2016).
- [7] L. E. Strigari, Dark matter in dwarf spheroidal galaxies and indirect detection: A review, *Rep. Prog. Phys.* **81**, 056901 (2018).
- [8] R. K. Leane, Indirect detection of dark matter in the galaxy, in *3rd World Summit on Exploring the Dark Side of the Universe* (University of Kansas Libraries Lawrence, Guadeloupe Islands, 2020), pp. 203–228, arXiv:2006.00513.
- [9] C. Pérez de los Heros, Status, challenges and directions in indirect dark matter searches, *Symmetry*, **12**, 1648 (2020).
- [10] W. H. Press and D. N. Spergel, Capture by the sun of a galactic population of weakly interacting, massive particles, *Astrophys. J.* **296**, 679 (1985).
- [11] A. Gould, Resonant enhancements in weakly interacting massive particle capture by the earth, *Astrophys. J.* **321**, 571 (1987).
- [12] A. Gould, Direct and indirect capture of weakly interacting massive particles by the earth, *Astrophys. J.* **328**, 919 (1988).
- [13] A. Gould, Gravitational diffusion of solar system wimps, *Astrophys. J.* **368**, 610 (1991).
- [14] J. Kumar, J. G. Learned, S. Smith, and K. Richardson, Tools for studying low-mass dark matter at neutrino detectors, *Phys. Rev. D* **86**, 073002 (2012).
- [15] R. Catena and B. Schwabe, Form factors for dark matter capture by the Sun in effective theories, *J. Cosmol. Astropart. Phys.* **04** (2015) 042.
- [16] A. Brenner, A. Ibarra, and A. Rappelt, Conservative constraints on the effective theory of dark matter-nucleon interactions from IceCube: The impact of operator interference, *J. Cosmol. Astropart. Phys.* **07** (2021) 012.
- [17] J. Silk, K. Olive, and M. Srednicki, The Photino, the Sun, and High-Energy Neutrinos, *Phys. Rev. Lett.* **55**, 257 (1985).
- [18] J. S. Hagelin, K. Ng, and K. A. Olive, A high-energy neutrino signature from supersymmetric relics, *Phys. Lett. B* **180**, 375 (1986).
- [19] M. Srednicki, K. A. Olive, and J. Silk, High-energy neutrinos from the sun and cold dark matter, *Nucl. Phys.* **B279**, 804 (1987).
- [20] G. Jungman and M. Kamionkowski, Neutrinos from particle decay in the sun and earth, *Phys. Rev. D* **51**, 328 (1995).
- [21] T. K. Gaisser, G. Steigman, and S. Tilav, Limits on cold-dark-matter candidates from deep underground detectors, *Phys. Rev. D* **34**, 2206 (1986).
- [22] G. Jungman, M. Kamionkowski, and K. Griest, Super-symmetric dark matter, *Phys. Rep.* **267**, 195 (1996).
- [23] S. Desai *et al.* (Super-Kamiokande Collaboration), Search for dark matter WIMPs using upward through-going muons in Super-Kamiokande, *Phys. Rev. D* **70**, 083523 (2004).
- [24] K. Choi *et al.* (Super-Kamiokande Collaboration), Search for Neutrinos from Annihilation of Captured Low-Mass Dark Matter Particles in the Sun by Super-Kamiokande, *Phys. Rev. Lett.* **114**, 141301 (2015).
- [25] M. G. Aartsen *et al.* (IceCube Collaboration), Search for annihilating dark matter in the Sun with 3 years of IceCube data, *Eur. Phys. J. C* **77**, 146 (2017).
- [26] A. M. Green, Astrophysical uncertainties on direct detection experiments, *Mod. Phys. Lett. A* **27**, 1230004 (2012).
- [27] N. Nagata and S. Shirai, Electroweakly-interacting dirac dark matter, *Phys. Rev. D* **91**, 055035 (2015).
- [28] R. Catena and F. Hellström, New constraints on inelastic dark matter from IceCube, *J. Cosmol. Astropart. Phys.* **10** (2018) 039.
- [29] M. McCullough and M. Fairbairn, Capture of inelastic dark matter in white dwarves, *Phys. Rev. D* **81**, 083520 (2010).
- [30] D. Hooper, D. Spolyar, A. Vallinotto, and N. Y. Gnedin, Inelastic dark matter as an efficient fuel for compact stars, *Phys. Rev. D* **81**, 103531 (2010).
- [31] R. Krall and M. Reece, Last electroweak WIMP standing: Pseudo-dirac higgsino status and compact stars as future probes, *Chin. Phys. C* **42**, 043105 (2018).
- [32] N. F. Bell, G. Busoni, and S. Robles, Heating up neutron stars with inelastic dark matter, *J. Cosmol. Astropart. Phys.* **09** (2018) 018.
- [33] M. Fujiwara, K. Hamaguchi, N. Nagata, and J. Zheng, Capture of electroweak multiplet dark matter in neutron stars, arXiv:2204.02238.
- [34] N. F. Bell, G. Busoni, M. E. Ramirez-Quezada, S. Robles, and M. Virgato, Improved treatment of dark matter capture in white dwarfs, *J. Cosmol. Astropart. Phys.* **10** (2021) 083.
- [35] N. F. Bell, G. Busoni, S. Robles, and M. Virgato, Improved treatment of dark matter capture in neutron stars, *J. Cosmol. Astropart. Phys.* **09** (2020) 028.
- [36] M. Cermeño and M. A. Pérez-García, Gamma rays from dark mediators in white dwarfs, *Phys. Rev. D* **98**, 063002 (2018).
- [37] M. Rotondo, J. A. Rueda, R. Ruffini, and S.-S. Xue, Relativistic feynman-metropolis-teller theory for white dwarfs in general relativity, *Phys. Rev. D* **84**, 084007 (2011).
- [38] C. Garcia-Cely and J. Heeck, Phenomenology of left-right symmetric dark matter, *J. Cosmol. Astropart. Phys.* **03** (2016) 021.
- [39] S. Ferrari, T. Hambye, J. Heeck, and M. H. G. Tytgat, SO (10) paths to dark matter, *Phys. Rev. D* **99**, 055032 (2019).
- [40] F. C. De Gerónimo, M. M. Miller Bertolami, F. Plaza, and M. Catelan, The composition of massive white dwarfs and their dependence on C-burning modeling, *Astron. Astrophys. J.* **659**, A150 (2022).
- [41] B. Dasgupta, A. Gupta, and A. Ray, Dark matter capture in celestial objects: Improved treatment of multiple scattering and updated constraints from white dwarfs, *J. Cosmol. Astropart. Phys.* **08** (2019) 018.
- [42] J. Reynoso-Cordova, M. Regis, and M. Taoso, Upper limits on the dark matter content in globular clusters, arXiv:2203.13735.

- [43] S. Mashchenko and A. Sills, Globular clusters with dark matter halos. I. Initial relaxation, *Astrophys. J.* **619**, 243 (2005).
- [44] G. Bertone and M. Fairbairn, Compact stars as dark matter probes, *Phys. Rev. D* **77**, 043515 (2008).
- [45] P. J. E. Peebles, Dark matter and the origin of galaxies and globular star clusters, *Astrophys. J.* **277**, 470 (1984).
- [46] S. Nussinov, L.-T. Wang, and I. Yavin, Capture of inelastic dark matter in the sun, *J. Cosmol. Astropart. Phys.* **08** (2009) 037.
- [47] A. Menon, R. Morris, A. Pierce, and N. Weiner, Capture and indirect detection of inelastic dark matter, *Phys. Rev. D* **82**, 015011 (2010).
- [48] J. Shu, P.-f. Yin, and S.-h. Zhu, Neutrino constraints on inelastic dark matter after CDMS II, *Phys. Rev. D* **81**, 123519 (2010).
- [49] R. Garani and S. Palomares-Ruiz, Dark matter in the Sun: Scattering off electrons vs nucleons, *J. Cosmol. Astropart. Phys.* **05** (2017) 007.
- [50] A. Bottino, G. Fiorentini, N. Fornengo, B. Ricci, S. Scopel, and F. L. Villante, Does solar physics provide constraints to weakly interacting massive particles?, *Phys. Rev. D* **66**, 053005 (2002).
- [51] N. Bernal, J. Martín-Albo, and S. Palomares-Ruiz, A novel way of constraining WIMPs annihilations in the Sun: MeV neutrinos, *J. Cosmol. Astropart. Phys.* **08** (2013) 011.
- [52] J. A. Formaggio and G. P. Zeller, From eV to EeV: Neutrino cross sections across energy scales, *Rev. Mod. Phys.* **84**, 1307 (2012).
- [53] www.marcocirelli.net/PPPC4DMID.html.
- [54] B. M. S. Hansen, H. B. Richer, G. G. Fahlman, P. B. Stetson, J. Brewer, T. Currie, B. K. Gibson, R. Ibata, R. Michael Rich, and M. M. Schara, HST observations of the white dwarf cooling sequence of M4, *Astrophys. J. Suppl. Ser.* **155**, 551 (2004).
- [55] L. R. Bedin, M. Salaris, G. Piotto, J. Anderson, I. R. King, and S. Cassisi, The end of the white dwarf cooling sequence in M4: An efficient approach, *Astrophys. J.* **697**, 965 (2009).
- [56] S. Chandrasekhar, The maximum mass of ideal white dwarfs, *Astrophys. J.* **74**, 81 (1931).
- [57] P. A. Mazzali, F. K. Ropke, S. Benetti, and W. Hillebrandt, A common explosion mechanism for type Ia supernovae, *Science* **315**, 825 (2007).
- [58] C. Kouvaris and P. Tinyakov, Constraining asymmetric dark matter through observations of compact stars, *Phys. Rev. D* **83**, 083512 (2011).
- [59] C. Kouvaris, WIMP annihilation and cooling of neutron stars, *Phys. Rev. D* **77**, 023006 (2008).
- [60] G. Busoni, Capture of dark matter in neutron stars, [arXiv:2201.00048](https://arxiv.org/abs/2201.00048).
- [61] S. Chatterjee, R. Garani, R. K. Jain, B. Kanodia, M. S. N. Kumar, and S. K. Vempati, Faint light of old neutron stars from dark matter capture and detectability at the James Webb Space Telescope, [arXiv:2205.05048](https://arxiv.org/abs/2205.05048).
- [62] M. Baryakhtar, J. Bramante, S. W. Li, T. Linden, and N. Raj, Dark Kinetic Heating of Neutron Stars and An Infrared Window On WIMPs, SIMPs, and Pure Higgsinos, *Phys. Rev. Lett.* **119**, 131801 (2017).
- [63] N. Raj, P. Tanedo, and H.-B. Yu, Neutron stars at the dark matter direct detection frontier, *Phys. Rev. D* **97**, 043006 (2018).
- [64] M. Cirelli, N. Fornengo, and A. Strumia, Minimal dark matter, *Nucl. Phys.* **B753**, 178 (2006).
- [65] J. Heeck and S. Patra, Minimal Left-Right Symmetric Dark Matter, *Phys. Rev. Lett.* **115**, 121804 (2015).
- [66] P. Duka, J. Gluza, and M. Zralek, Quantization and renormalization of the manifest left-right symmetric model of electroweak interactions, *Ann. Phys. (N.Y.)* **280**, 336 (2000).
- [67] J. C. Romao and J. P. Silva, A resource for signs and Feynman diagrams of the Standard Model, *Int. J. Mod. Phys. A* **27**, 1230025 (2012).
- [68] A. L. Fitzpatrick, W. Haxton, E. Katz, N. Lubbers, and Y. Xu, The effective field theory of dark matter direct detection, *J. Cosmol. Astropart. Phys.* **02** (2013) 004.
- [69] F. Bishara, J. Brod, B. Grinstein, and J. Zupan, From quarks to nucleons in dark matter direct detection, *J. High Energy Phys.* **11** (2017) 059.
- [70] I. Jeong, S. Kang, S. Scopel, and G. Tomar, WimPyDD: An object-oriented Python code for the calculation of WIMP direct detection signals, *Comput. Phys. Commun.* **276**, 108342 (2022).
- [71] G. Tomar, I. Jeong, S. Kang, and S. Scopel, WimPyDD: An object-oriented Python code for WIMP-nucleus scattering direct detection in virtually any scenario, *J. Phys. Conf. Ser.* **2156**, 012061 (2021).
- [72] M. Aaboud *et al.* (ATLAS Collaboration), Search for a right-handed gauge boson decaying into a high-momentum heavy neutrino and a charged lepton in pp collisions with the ATLAS detector at $\sqrt{s} = 13$ TeV, *Phys. Lett. B* **798**, 134942 (2019).
- [73] G. Chauhan, P. S. B. Dev, R. N. Mohapatra, and Y. Zhang, Perturbativity constraints on $U(1)_{B-L}$ and left-right models and implications for heavy gauge boson searches, *J. High Energy Phys.* **01** (2019) 208.
- [74] N. D. Christensen and C. Duhr, FeynRules—Feynman rules made easy, *Comput. Phys. Commun.* **180**, 1614 (2009).
- [75] A. Roitgrund, G. Eilam, and S. Bar-Shalom, Implementation of the left-right symmetric model in FeynRules, *Comput. Phys. Commun.* **203**, 18 (2016).
- [76] A. Belyaev, N. D. Christensen, and A. Pukhov, CalcHEP 3.4 for collider physics within and beyond the Standard Model, *Comput. Phys. Commun.* **184**, 1729 (2013).
- [77] G. Bélanger, F. Boudjema, A. Goudelis, A. Pukhov, and B. Zaldivar, micrOMEGAs5.0: Freeze-in, *Comput. Phys. Commun.* **231**, 173 (2018).
- [78] J. C. Pati and A. Salam, Lepton number as the fourth color, *Phys. Rev. D* **10**, 275 (1974).
- [79] T. W. B. Kibble, G. Lazarides, and Q. Shafi, Walls bounded by strings, *Phys. Rev. D* **26**, 435 (1982).
- [80] T. G. Rizzo and G. Senjanovic, Grand unification and parity restoration at low-energies. 2. Unification constraints, *Phys. Rev. D* **25**, 235 (1982).
- [81] T. G. Rizzo and G. Senjanovic, Grand unification and parity restoration at low-energies. 1. Phenomenology, *Phys. Rev. D* **24**, 704 (1981).
- [82] R. N. Mohapatra and G. Senjanovic, Neutrino masses and mixings in gauge models with spontaneous parity violation, *Phys. Rev. D* **23**, 165 (1981).

- [83] N. G. Deshpande, J. F. Gunion, B. Kayser, and F. I. Olness, Left-right symmetric electroweak models with triplet Higgs, *Phys. Rev. D* **44**, 837 (1991).
- [84] N. T. Shaban and W. J. Stirling, Minimal left-right symmetry and SO(10) grand unification using LEP coupling constant measurements, *Phys. Lett. B* **291**, 281 (1992).
- [85] Y. Mambrini, N. Nagata, K. A. Olive, J. Quevillon, and J. Zheng, Dark matter and gauge coupling unification in nonsupersymmetric SO(10) grand unified models, *Phys. Rev. D* **91**, 095010 (2015).
- [86] J. Chakraborty, R. Maji, S. K. Patra, T. Srivastava, and S. Mohanty, Roadmap of left-right models based on GUTs, *Phys. Rev. D* **97**, 095010 (2018).
- [87] E. J. Chun and L. Velasco-Sevilla, Tracking down the route to the SM with inflation and gravitational waves, *Phys. Rev. D* **106**, 035008 (2022).
- [88] M. Lindner and M. Weiser, Gauge coupling unification in left-right symmetric models, *Phys. Lett. B* **383**, 405 (1996).
- [89] Y. Aoki, T. Izubuchi, E. Shintani, and A. Soni, Improved lattice computation of proton decay matrix elements, *Phys. Rev. D* **96**, 014506 (2017).
- [90] K. Abe *et al.* (Super-Kamiokande Collaboration), Search for proton decay via $p \rightarrow e^+\pi^0$ and $p \rightarrow \mu^+\pi^0$ in 0.31 megaton \cdot years exposure of the Super-Kamiokande water Cherenkov detector, *Phys. Rev. D* **95**, 012004 (2017).
- [91] K. Abe *et al.* (Hyper-Kamiokande Collaboration), Hyper-kamiokande design report, [arXiv:1805.04163](https://arxiv.org/abs/1805.04163).
- [92] L. Sartore and I. Schienbein, PyR@TE 3, *Comput. Phys. Commun.* **261**, 107819 (2021).
- [93] J. Chakraborty, R. Maji, and S. F. King, Unification, proton decay and topological defects in non-SUSY GUTs with thresholds, *Phys. Rev. D* **99**, 095008 (2019).